The Geological Society of America
Special Paper 515
2015

Modern muds of Laguna Mar Chiquita (Argentina): Particle size and organic matter geochemical trends from a large saline lake in the thick-skinned Andean foreland

Michael M. McGlue*
Central Energy Resources Science Center, U.S. Geological Survey, Denver Federal Center, MS 977, P.O. Box 25046, Denver, Colorado 80225, USA, and
Department of Earth and Environmental Sciences, University of Kentucky, Lexington, Kentucky 40506, USA

Geoffrey S. Ellis
Central Energy Resources Science Center, U.S. Geological Survey, Denver Federal Center, MS 977, P.O. Box 25046, Denver, Colorado 80225, USA

Andrew S. Cohen
Department of Geosciences, University of Arizona, 1040 E. 4th Street, Tucson, Arizona 85721, USA

ABSTRACT

Laguna Mar Chiquita (central Argentina; ~latitude 31°S, longitude 63°W) provides an outstanding opportunity to examine organic facies development and petroleum source-rock potential in a modern thick-skinned foreland basin lake. In this case study, we define profundal, paleodelta, and lake-margin depositional environments based on trends in bathymetry and lake-floor sediment particle size. Sedimentary geochemical analyses indicate that organic carbon–rich muds accumulate in profundal environments during the extant lake-level highstand. The lateral variability of organic facies is minimal. The quality of organic facies is controlled by lake level and depositional environment, both of which dictate patterns of algal productivity, siliciclastic dilution, and early diagenesis. We present conceptual models of lacustrine source rocks in both thick-skinned and thin-skinned foreland basins based on modern analog data from both Laguna Mar Chiquita and other lakes in the central Andean foreland. Over relatively short time intervals (10^2–10^4 yr), climatically driven water-level fluctuations influence the source-rock potential of these basins. Over time intervals >10^5 yr, contraction and lateral migration of the basin flexural profile control stratal stacking patterns and the potential for hydrocarbon play development.

*michael.mcglue@uky.edu

McGlue, M.M., Ellis, G.S., and Cohen, A.S., 2015, Modern muds of Laguna Mar Chiquita (Argentina): Particle size and organic matter geochemical trends from a large saline lake in the thick-skinned Andean foreland, *in* Larsen, D., Egenhoff, S.O., and Fishman, N.S., eds., Paying Attention to Mudrocks: Priceless!: Geological Society of America Special Paper 515, doi:10.1130/2015.2515(01).

INTRODUCTION

Ancient lake systems associated with thick-skinned foreland basins (e.g., broken foreland basins of Jordan, 1995; Laramide sedimentary basins of Lawton, 2008) developed some of the most economically important sedimentary deposits in North America. This is particularly true of the Eocene Green River Formation of the western United States (e.g., Eugster and Hardie, 1975; Roehler, 1993; Smith et al., 2008). Dubiel (2003), for example, noted the importance of Green River Formation source rocks to both conventional oil (e.g., the Altamont-Bluebell field reservoirs) and unconventional tar sands prospects in the Uinta Basin of Utah. Recent assessments of in-place oil shale for the Green River Formation of the Greater Green River, Uinta, and Piceance Basins indicate a vast resource base of ~4.3×10^{12} barrels of oil in place (Johnson et al., 2011). The thick, cyclic strata of the Wilkins Peak Member, a saline-lake phase in the Green River Formation, exclusively accounts for >700×10^{9} barrels of oil in the Greater Green River Basin (Johnson et al., 2011). In addition, lacustrine coal beds with the potential for unconventional methane accumulations are present throughout the Greater Green River and Uinta Basins (Roberts, 2005). Saline-lacustrine deposits from the Green River Formation have also been exploited for sodium carbonates (e.g., nahcolite and trona) that have numerous commercial uses, including soda ash production, air and water pollution control, animal feed, detergents, cement production, glass manufacturing, and a host of medical applications (Dyni, 1996; Santini et al., 2006; Brownfield et al., 2010). More generally, the source of many base-metal and oil resources in China, Australia, and North America are thought to have been saline-lake environments (e.g., Smoot and Lowenstein, 1991).

South America provides a rich natural laboratory for the study of modern foreland basin saline lakes and their muds (Cohen et al., 2014). The central Andean retroarc foreland basin (Horton and DeCelles, 1997) is a classic, four-part, thin-skinned system composed of wedgetop, foredeep, forebulge, and back-bulge depozones (DeCelles and Giles, 1996), as well as vast regions of sediment accumulation in the high-altitude hinterland (Horton, 2011). Saline and brackish lakes are common in hinterland basins and in areas of the back-bulge (e.g., Wirrmann and Mourguiart, 1995; Valero-Garcés et al., 2000; Furquim et al., 2008; McGlue et al., 2012). In the southern Andean foreland, Laramide-style deformation in the Miocene and Pliocene (Jordan and Allmendinger, 1986; Kay and Abbruzzi, 1996) led to the development of thick-skinned foreland basins adjacent to or between basement-cored uplifts. A number of large saline lakes or playas occupy these basins today, including Salina de Ambargasta, Salinas Grandes, and Laguna Mar Chiquita (e.g., Dargám, 1994; Piovano et al., 2002; Zanor et al., 2012).

In this case study we report on the lake-floor sediments of Laguna Mar Chiquita (LMC; also referred to by some as Mar de Ansenuza), one of the best modern analogs available for ancient saline lakes in a thick-skinned foreland basin setting. Most of the geological research on LMC to date has focused on basin-scale geomorphology, hydrogeology, and paleoclimate (e.g., Piovano et al., 2004; Mon and Gutiérrez, 2009; Troin et al., 2010). Comprehensive sedimentological and geochemical data sets from LMC are scarce, and the research presented herein attempts to build upon initial work published earlier (Martínez, 1995). Kröhling and Iriondo (1999) developed a useful Quaternary geological map of the LMC region through analysis of onshore landforms and stratigraphy; however, geological details from the offshore remain limited. Our work aims to provide the first basin-wide characterization of detrital particle size and organic matter geochemistry for the modern muds of LMC. Huc et al. (1990) noted the importance of lateral variations in sediment fabric and organic richness to lacustrine petroleum source rocks. We investigated the relationships among depositional environments and organic facies in LMC, with a goal of improving hydrocarbon exploration models in continental foreland settings.

TECTONIC SETTING

Laguna Mar Chiquita shares a broadly similar tectonic heritage to some of the large lakes associated with Laramide deformation in the western United States (e.g., the Eocene Green River Formation; Eugster and Hardie, 1975; Surdam and Stanley, 1979; Jordan and Allmendinger, 1986). The lake is located in the Pampean plains of central Argentina (~latitude 31°S, longitude 63°W; Fig. 1A). Laguna Mar Chiquita occupies a topographically closed basin in the eastern Sierras Pampeanas, an area well known in the southern Andes for its flat-slab subduction (Jordan and Allmendinger, 1986; Cahill and Isacks, 1992; Ramos et al., 2002; Gans et al., 2011). To the west of the lake, the basement-cored Sierras de Córdoba formed from westward-verging thrust faults (Fig. 1B). To the east, a buried westward-verging thrust fault, the Tostado-Selva fault, forms a broad topographic swell known as the San Guillermo High (Fig. 1B). This feature is believed to have impounded the southward-flowing Río Dulce and eastward-flowing Ríos Primero and Segundo, thus helping to form LMC. Mon and Gutiérrez (2009) speculated that hydrologic capture and lake formation occurred in the middle Pleistocene, but there are no absolute geochronology data, and age constraints are limited to regional correlations. Pelletier (2007) suggested that LMC is within the wedgetop depozone of this broken foreland, as the western lake margin is <150 km from the thrust front. Dávila et al. (2010) suggested that the lake occupies a position in the distal foredeep of a thick-skinned foreland, produced by the interplay of loading by the Sierras de Córdoba in the Miocene and loading induced by a dynamic flat slab.

HYDROLOGY AND LIMNOLOGY

Laguna Mar Chiquita is a hydrologically closed, underfilled lake basin (rates of potential accommodation continually exceed the rate of sediment plus water infill; Carroll and Bohacs, 1999). The catchment of LMC is very large (>37,000 km^2), and the most important surface water and solute input to the lake is the

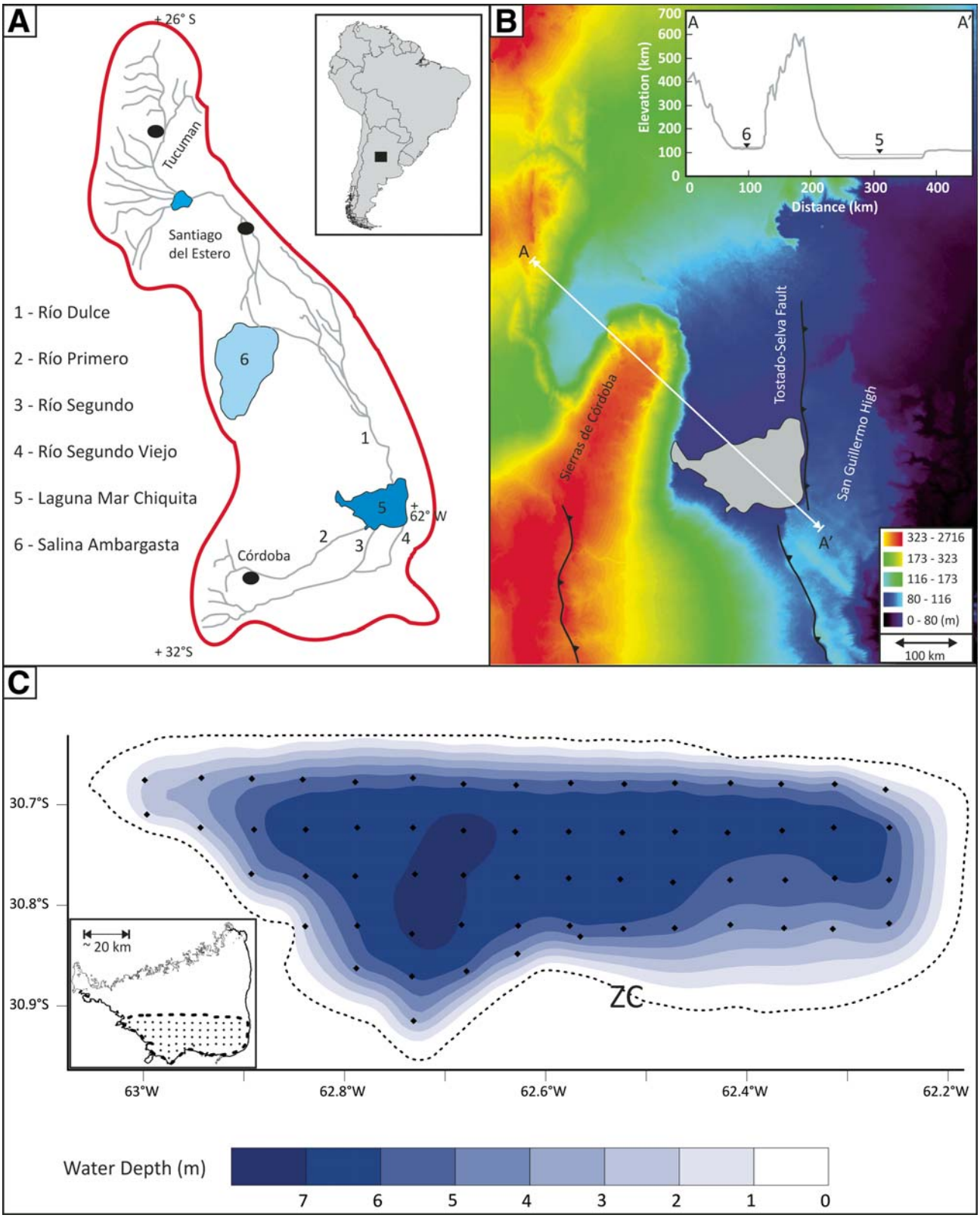

Figure 1. (A) Laguna Mar Chiquita (LMC) and its watershed in central Argentina. Inset map shows the position of the catchment in South America. (B) Shuttle Radar Topography Mission (90 m) digital elevation model of the thick-skinned foreland basin that contains LMC and surrounding ranges and basins. Transect A-A′ illustrates the topography adjacent to the lake; numbers correspond to features labeled in A. (C) Surface sediment sample map (dots) and calculated bathymetry for LMC. Contour interval is 1 m. Inset map illustrates recent highstand shoreline and the location of the sample grid. The northern end of the lake, which was only recently formed by flooding of the Río Dulce, was not sampled. The lake basin reaches maximum depth of ~7 m. ZC—zero contour.

Río Dulce (Martínez, 1995; Troin et al., 2010). North of LMC, the Río Dulce incorporates tributaries from portions of Salina de Ambargasta, which can act as an open-hydrologic system under certain climatic conditions (Zanor et al., 2012; Fig. 1A). The Sierras de Córdoba forms the headwater region for the Ríos Primero and Segundo, two key rivers that enter LMC from the south (Fig. 1A); these rivers are also known as the Ríos Susquía and Xanaes, respectively. Another river channel, the Río Segundo Viejo, interacts with the southern shoreline, but discharge to the lake is limited due to anthropogenic engineering (Kröhling and Iriondo, 1999; Fig. 1A). Although the extent of its contribution is still unknown, groundwater is believed to play an important role in maintaining the water balance of LMC (Reati et al., 1996; Troin et al., 2010).

The terminal Río Dulce wetlands, which currently form the northern end of the lake, developed as a result of a dramatic transgression in the 1970s. As a consequence, the surface area of LMC today is much larger than in the recent past. The lake surface elevation is at ~70 m above sea level (a.s.l.) and is juxtaposed with the San Guillermo High, which is adjacent to the lake's eastern margin at 100 m a.s.l. Reati et al. (1996) reported a maximum water depth (Z_{max}) of 8.6 m and an average depth (Z_{ave}) of 3.7 m, whereas Piovano et al. (2002) reported a Z_{max} of 10 m. The Z_{max} we encountered in the field was 7.0 m (Z_{ave} = 5.9 m; Fig. 1C). Based on the bathymetric map of Reati et al. (1996), it is highly likely that our survey covered the deepest part of the basin, which implies that annual-decadal bathymetric variations of as much as ~3 m may characterize LMC, perhaps in response to prevailing conditions of effective precipitation and river discharge. Multiple measurements of pH taken from the southern lake shoreline during our 2008 survey averaged 8.2. Surface-water chemical assessments conducted by Martínez (1995) indicated a Na^{2+}-Cl^{-}-SO_4^{2-} brine type and no evidence of thermal stratification. Thus, the lake is believed to be polymictic. Reati et al. (1996) indicated that persistent winds affect LMC and fair-weather waves as high as 0.4 m were common offshore, potentially preventing water-column stratification. Prior to the 1970s transgression, values of salinity for LMC ranged between 251 and 360 g/L (Martínez, 1995; Reati et al., 1996). Salinity values reflecting the highstand lake-level condition ranged from 29 to 35 g/L (Martínez et al., 1994). Vegetation associated with the lake is not well described in the literature, but both Reati et al. (1996) and Varandas da Silva et al. (2008) documented various species of the macrophyte *Ruppia* growing in sheltered lake-margin environments.

CLIMATE

Using the Köppen-Geiger climate system, LMC and its catchment are within the temperate Cwa and Cfa classes (Peel et al., 2007). Summers are generally warm and wet, with average temperatures above 20 °C between November and March (Vörösmarty et al., 1998); winters are cool and dry with average temperatures of ~13 °C from April and October. The average annual temperature is 17–18 °C. Precipitation is strongly seasonal and station records from Córdoba (1963–1989), where complete, show that mean annual rainfall is 814 mm (Vörösmarty et al., 1998). Additional precipitation data from Santa Fe province (1981–1990; http://www.smn.gov.ar) indicate mean annual rainfall of ~942 mm/yr in the lowlands northeast of LMC. A number of studies indicate that strong variability in total rainfall has characterized the historic period, and the annual average rainfall prior to 1973 was ~653 mm (Genta et al., 1998; Piovano et al., 2004). Surface area data for LMC reflect this variability and range from 2000 km^2 to 6000 km^2 (Troin et al., 2010). Values of potential evapotranspiration in the region vary, but in all cases exceed total annual precipitation, indicating a negative hydrologic balance (Reati et al., 1996).

METHODS

Lake-floor sediment samples (n = 61) were collected from southern LMC in a grid pattern using a Ponar-style dredge. Our survey focused on southern LMC because this area has most likely been the main site of lacustrine deposition in the late Quaternary. The diffuse and shallow northern end of LMC is essentially a forest that drowned due to recent Río Dulce flooding. This region is extremely difficult to navigate safely and therefore we excluded it from the survey. The spacing between our sample sites was typically ≤5 km (Fig. 1C). Water depth was measured at each site using a hand-held sonar device. For the purpose of classification, all samples <10 km from the shoreline (water depths <6 m) were defined as nearshore. Samples classified as offshore were typically found >10 km from the shoreline in deeper water. The upper ~1 cm of each grab sample was transferred into labeled storage jars in the field and shipped to the United States for analysis.

Upon arrival in the lab, samples were homogenized and split. A representative subset of samples was analyzed by microscopic examination of 125 µm screen-washed residues and smear slides to obtain qualitative insights on sedimentary components. The mineralogy of a subset of samples (n = 25) was investigated by bulk powder X-ray diffraction (XRD) following the analytical protocol of Eberl (2003). Clay mineralogy was verified using the techniques outlined in Moore and Reynolds (1989). All samples were evaluated for particle size and sedimentary geochemistry using standard techniques, with a special focus on organic matter (OM) geochemistry. Sample splits for particle size analysis, total inorganic carbon (TIC), biogenic silica (BiSi), and Rock-Eval pyrolysis were prepared following the procedures discussed in McGlue et al. (2012). Sample preparation and analysis for total nitrogen (TN) and bulk $\delta^{15}N$ assays followed the procedures described in McGlue et al. (2011). Nitrogen isotope values reported herein use the conventional delta notation relative to atmospheric nitrogen. The precision of the nitrogen isotope analysis was typically better than ~0.2‰. Total organic carbon (TOC) was calculated as the weight difference between total carbon and TIC, determined using a UIC Inc. total carbon coulometer at the University of Minnesota. Analytical precision associated with the

technique was ~0.2%. Carbon isotopes were measured on OM at the U.S. Geological Survey using an Optima isotope ratio mass spectrometer coupled with an elemental analyzer. Carbon isotope values reported herein use the conventional delta notation relative to Vienna Peedee belemnite. The precision was ~0.07‰ based on repeated analysis of internal standards. In order to remove carbonates that could influence the $\delta^{13}C_{OM}$ results, samples were acidified using 20% HCl for 24 h prior to analysis. Reported weight percent total organic nitrogen (TON) and C/N values reflect only OM, as contributions from inorganic-bound N were estimated and corrected using the technique described by Talbot (2001).

Contour maps of particle size and geochemistry were created using the radial basis gridding function of Surfer v. 8.05 (Golden Software Inc.; www.goldensoftware.com). We imposed a zero contour that was defined by the position of the southern lake shoreline and the sample grid. This exercise closes contours and improves the quality of the maps, but it also introduces error in the form of spuriously low values along the margins of the sample grid. Ternary diagrams and cross plots were developed using SigmaPlot v. 12 (Systat Software Inc.; www.sigmaplot.com).

RESULTS AND INTERPRETATIONS

Detrital Particle Size

Results

Using the nomenclature of Folk (1980), the majority of LMC modern sediments, regardless of water depth, plot within the mud texture class (Table 1; Fig. 2A). The ratio of silt to clay of mud-class samples varied from 0.6 to 1.8, and a histogram of silt:clay shows that clay sizes (<3.9 µm) predominate (Fig. 2B). XRD analyses indicate that clay minerals in the majority of samples consist of abundant illite, with lesser amounts of calcium-rich smectite and minor to trace amounts of kaolinite (Fig. 2C). Coarse grain sizes are uncommon (<3.0%) in mud-class samples; however, terrigenous sand is abundant in samples trending offshore from the mouth of the Río Segundo Viejo (Figs. 3 and 4A). The texture classes of these samples range from sand to sandy silt, and D_{90} values (125–880 µm) indicate that maximum particle sizes are in the fine to coarse sand range (Wentworth, 1922; Fig. 2A). X-ray diffraction indicates that the mineralogy of these sands consists of quartz, plagioclase, volcanic glass, and micas. Sandy and silty sediments were also encountered at nearshore (<6 m water depth; Fig. 4A) sites along the western boundary of the sample grid.

Interpretations

Coupled with bathymetric data, we interpret the spatial distribution of sand, silt, and clay contours to signify the presence of two profundal environments of deposition (EOD) separated by a relatively narrow, north-south–oriented shoal (Figs. 3, 4A, 4B, and 4C). The main profundal EOD, on the western side of the sample grid, is large (~650 km^2) and characterized by relatively deep water, whereas the eastern profundal EOD is smaller and shallower (Fig. 3). Clay concentration is highest (silt:clay < 0.7) in the west; we attribute this to sedimentation dominated by suspension-settling processes (Fig. 4C). We interpret the shoal between the profundal EODs as a paleodelta deposit, and sand with gastropod shell hash associated with this environment covers at least 70 km^2. We favor a deltaic interpretation because of the wedge shape exhibited by percent sand contours and the location near the mouth of the Río Segundo Viejo (Figs. 3 and 4A). The Río Segundo Viejo no longer contains active channels, due to a canalization project that was completed in 1930 (Kröhling and Iriondo, 1999). This suggests that the delta is a relict feature that is not actively aggrading or prograding. The bathymetric map of Reati et al. (1996) suggests that both subaerial and subaqueous deltaic features are likely to be encompassed by our percent sand and percent silt contours. Areas adjacent to the northern end of the shoal in both profundal EODs show elevated concentrations of detrital silt (Fig. 4B). Given this particle size pattern, we cannot discount the possibility that this feature is a sand spit, generated by littoral drift. Anecdotal evidence suggests that a westward littoral current impacts the southern lake shore; however, the results of an experiment designed to confirm the presence of the current were inconclusive (Reati et al., 1996).

Sandy and silty sediments found along the western margin of LMC are likely associated with the dune field described in Kröhling and Iriondo (1999), according to whom deflation of the Río Primero and Río Segundo floodplains during the Little Ice Age carpeted the western margin of LMC with fine eolian sands (Campo Maare Formation). Where exposed onshore, the dunes vary in height to as high as ~4 m (Kröhling and Iriondo, 1999). Our sampling grid was too coarse to fully resolve the bathymetric expression of the submerged dune field, and it is likely that these features would be heavily reworked by wave action. Nevertheless, the high silt concentration along the western edge of the sample grid (Fig. 4B) hint at the presence of these eolian deposits.

TIC and BiSi

Results

Values of TIC range from 0.13 to 1.74 wt%, with a mean of 0.97 wt% at nearshore sampling sites; offshore the range expands from 0.01 to 2.33 wt% and the mean increases to 1.33 wt% (see Table 2). Contours of TIC appear to show that concentration increases with distance from the southern lake shore, reaching maximum values in the western profundal EOD (Fig. 4D). However, TIC > 1.0 wt% spans all EODs where water depths exceed 6 m. X-ray diffraction data indicate that calcite is the dominant carbonate mineralogy, which is consistent with the findings of earlier studies (Martínez, 1995).

Analyses of screen-washed samples identified carbonate ostracode carapaces, foraminiferan tests, and gastropod shells. The gastropods consist of the high-spired *Littoridina parchappei*, which are abundant in samples from the paleodelta EOD. A single, minute gastropod (4–5 mm long; globose shell form) was also encountered, but taphonomic damage prevented identification. The ostracodes

TABLE 1. LAGUNA MAR CHIQUITA SURFACE SAMPLE LOCATIONS, DEPTH, AND DETRITAL PARTICLE SIZE DATA

Sample	Latitude (°S)	Longitude (°W)	Depth (m)	Mean particle size (μm)	Clay (%)	Silt (%)	Sand (%)
MC 01	30.865	62.674	6.4	7.7	53.7	45.9	0.4
MC 02	30.819	62.679	6.8	5.1	59.7	40.1	0.3
MC 03	30.770	62.677	6.9	7.5	47.8	52.1	0.1
MC 04	30.726	62.677	6.9	7.8	N.D.	N.D.	N.D.
MC 05	30.680	62.677	6.4	8.4	42.4	57.5	0.1
MC 06	30.681	62.625	6.2	7.9	43.6	56.0	0.4
MC 07	30.727	62.626	6.7	5.6	57.2	42.7	0.1
MC 08	30.772	62.624	6.5	6.5	53.1	46.8	0.1
MC 09	30.820	62.623	6.1	10.7	45.5	52.7	1.8
MC 10	30.849	62.623	4.7	74.9	8.4	43.1	48.4
MC 11	30.914	62.728	5.4	8.1	46.3	53.5	0.2
MC 12	30.870	62.728	6.6	5.9	59.5	40.5	0.1
MC 13	30.828	62.728	7.0	4.7	62.9	37.0	0.1
MC 14	30.769	62.725	6.9	5.3	60.0	39.9	0.1
MC 15	30.723	62.727	6.8	6.0	50.0	49.9	0.1
MC 16	30.674	62.727	6.2	6.6	48.1	51.8	0.1
MC 17	30.678	62.784	6.3	6.9	46.8	53.1	0.1
MC 18	30.723	62.782	6.4	4.6	60.8	39.1	0.1
MC 19	30.771	62.784	6.7	6.9	58.8	40.7	0.5
MC 20	30.820	62.782	6.2	4.4	64.5	35.1	0.4
MC 21	30.862	62.783	6.0	4.9	61.9	38.0	0.1
MC 23	30.820	62.834	3.6	387.3	3.1	18.1	78.9
MC 24	30.771	62.833	6.1	18.0	53.3	44.9	1.8
MC 25	30.725	62.833	6.3	4.4	62.6	37.4	0.0
MC 26	30.674	62.836	5.8	8.7	47.3	52.1	0.6
MC 27	30.674	62.887	5.2	7.4	56.4	42.8	0.8
MC 28	30.725	62.884	5.9	5.8	53.1	47.0	0.1
MC 29	30.768	62.886	5.6	6.0	54.6	45.4	0.1
MC 30	30.723	62.937	3.9	33.7	38.8	46.0	15.2
MC 31	30.674	62.936	3.8	6.6	54.9	45.0	0.1
MC 32	30.675	62.992	3.0	15.4	37.2	59.8	3.0
MC 33	30.709	62.990	4.1	9.1	45.7	53.9	0.5
MC 34	30.831	62.562	5.8	13.4	38.3	60.2	1.5
MC 34A	30.820	62.572	6.2	13.2	38.9	59.5	1.6
MC 35	30.773	62.573	6.5	9.5	42.2	57.7	0.1
MC 36	30.727	62.573	6.6	12.2	35.6	64.2	0.2
MC 37	30.679	62.571	6.2	12.9	34.6	64.7	0.7
MC 38	30.680	62.518	6.3	27.0	13.1	83.7	3.1
MC 39	30.728	62.520	6.6	6.0	55.7	44.2	0.1
MC 40	30.774	62.522	6.6	10.0	44.7	54.5	0.8
MC 41	30.823	62.519	6.1	9.5	42.6	57.1	0.3
MC 42	30.823	62.469	5.6	32.1	19.7	64.5	15.8
MC 43	30.777	62.470	6.5	9.6	42.2	57.5	0.3
MC 44	30.727	62.468	6.6	10.5	41.2	58.1	0.7
MC 45	30.679	62.468	6.4	21.9	23.4	72.7	4.0
MC 47	30.819	62.413	4.2	99.2	5.9	28.5	65.6
MC 48	30.775	62.413	5.5	103.2	1.5	27.8	70.8
MC 49	30.728	62.416	6.6	253.0	2.6	6.4	91.0
MC 50	30.679	62.413	6.2	300.0	5.8	9.9	84.3
MC 52	30.822	62.361	4.4	77.6	2.0	43.4	54.6
MC 53	30.776	62.359	5.9	42.1	N.D.	N.D.	N.D.
MC 54	30.726	62.362	6.5	11.9	39.3	59.8	0.9
MC 55	30.680	62.363	6.2	36.0	36.8	60.8	2.4
MC 56	30.680	62.310	6.2	30.8	25.4	71.1	3.5
MC 57	30.723	62.311	6.3	20.9	16.3	62.4	21.4
MC 58	30.773	62.310	6.1	8.1	52.2	47.0	0.7
MC 59	30.823	62.313	3.1	77.3	5.7	59.1	35.3
MC 62	30.818	62.256	4.9	6.1	54.5	45.4	0.2
MC 63	30.774	62.257	5.8	7.5	46.5	53.4	0.1
MC 64	30.723	62.256	6.1	7.2	50.3	49.6	0.1
MC 65	30.680	62.257	6.0	14.8	N.D.	N.D	N.D

N.D.—no data.

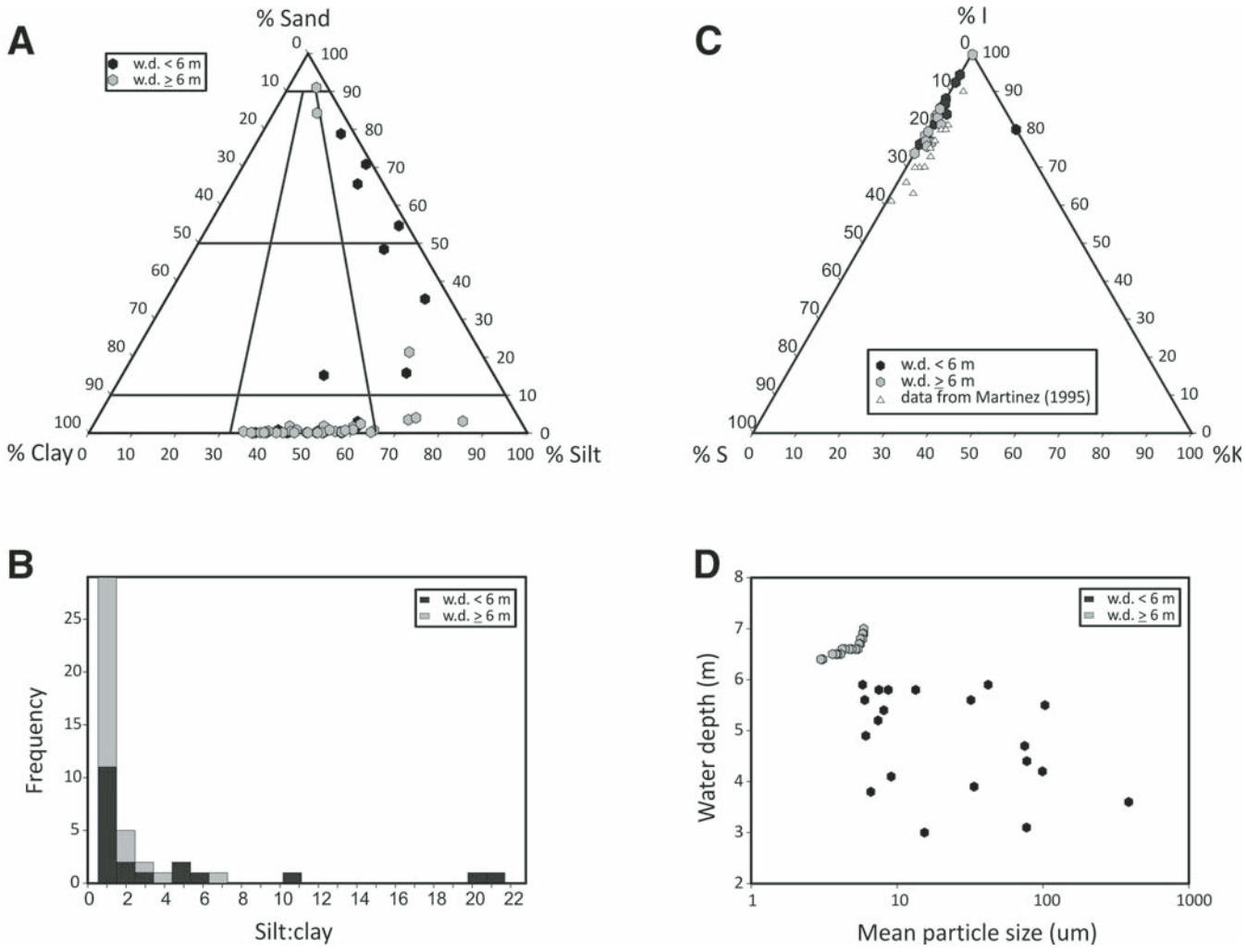

Figure 2. Detrital particle size and clay mineralogy of Laguna Mar Chiquita (LMC) surface samples. (A) Particle-size ternary diagram (after Folk, 1980). The majority of the samples are within the mud texture class (w.d.—water depth). (B) Histogram of detrital silt:clay, which illustrates the predominance of clay-sized particles in offshore mud-class samples. (C) Ternary diagram of normalized clay mineralogy calculated from X-ray diffraction patterns. I—illite, S—smectite, K—kaolinite. Illite is the most abundant clay mineral in LMC, which could be significant for unconventional gas storage. (D) Semi-log cross-plot of water depth (m) versus mean particle size (μm). Note the tight cluster of fine-grained samples in the offshore environment, whereas nearshore samples exhibit greater variability and generally much coarser sizes.

consist of two species: *Cyprideis salebrosa* (very common) and an unidentified and possibly new species of *Limnocythere* (rare). A single foraminifera species, *Ammonia beccari* (K. McDougall-Reid, 2012, personal commun.), was also present.

Values of BiSi range from 0.0 to 6.0 wt%, with a mean of 4.1 wt% at nearshore sites. Farther offshore (water depth > 6 m), the concentration of BiSi is similar, with a range of 0.0–7.8 wt% and a mean of 4.1 wt%. The arrangement of BiSi contours broadly follows depositional environment and decreases with proximity to the shoreline (Fig. 4E).

Interpretations

In addition to the authigenic carbonate deposition reported by Piovano et al. (2004), our results document important contributions to LMC sedimentary TIC from benthic biogenic sources. Although only two species of ostracodes were found, depauperate assemblages of this kind are not unusual for saline lakes. Nonmarine occurrences of the foraminifera *Ammonia beccari* have been documented on several continents, and usually result from avian introduction or ephemeral incursions of seawater (e.g., Cann and De Deckker, 1981). Laguna Mar Chiquita is a well-known rookery and seasonal habitat for shorebirds, which may explain the presence of this foraminifera (Nores, 2011). An alternative means of introduction is linked to human activities, such as from boats or through the development of the lake's pejerrey (*Odontesthes bonariensis*) sport fishery.

The presence of diatoms on smear slides suggests that they are the dominant source of BiSi. While limited information is

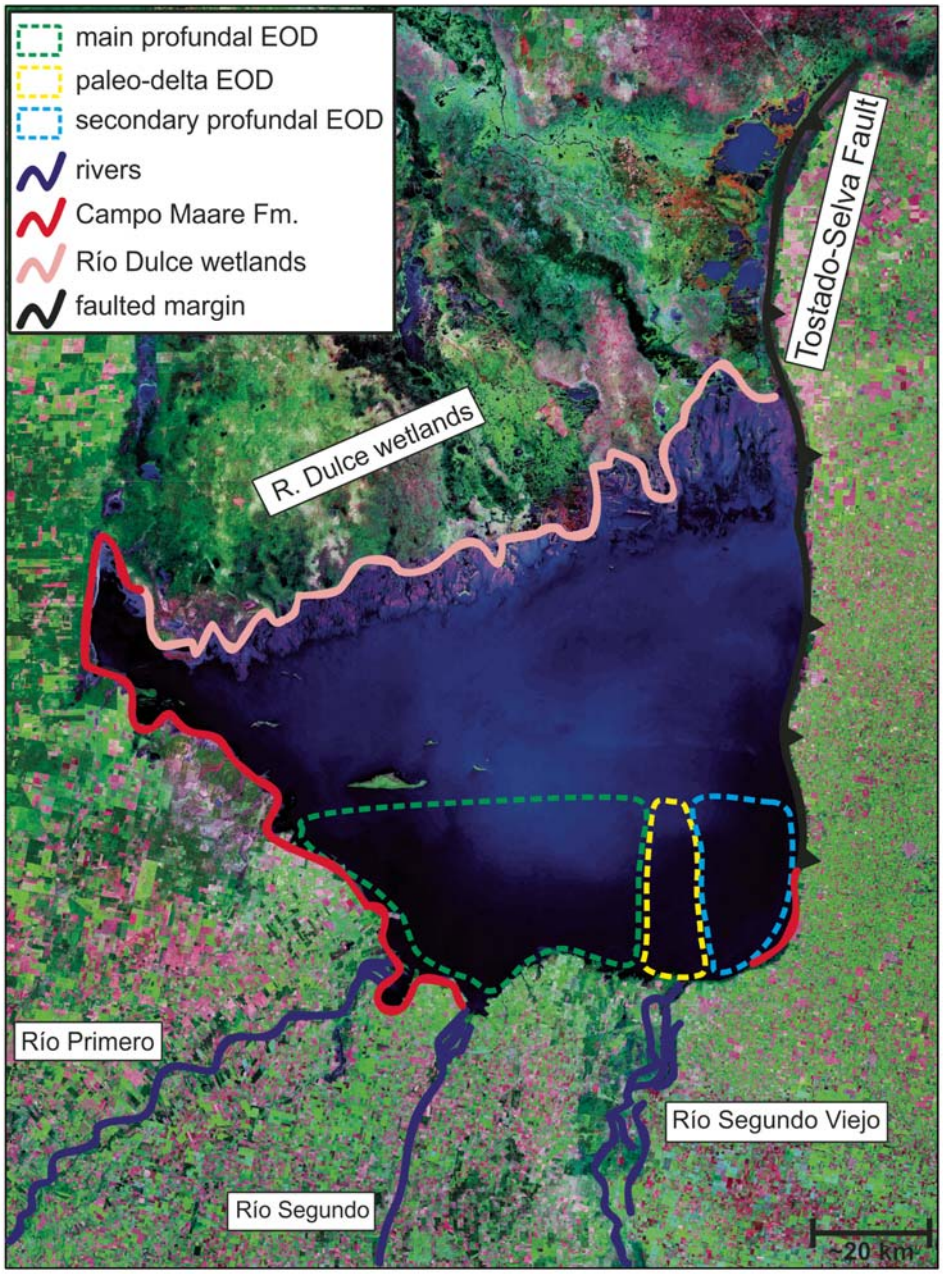

Figure 3. Gross depositional environments of Laguna Mar Chiquita. Base map is a MrSid Geocover2000 satellite image product (available from http://zulu.ssc.nasa.gov/mrsid/). Onshore and marginal environments and stratigraphy were described in Kröhling and Iriondo (1999). Bathymetric and particle size data were used to define profundal and paleodelta environments of deposition (EOD). Fm.—formation.

available about the distribution of the diatom flora in the lake, the census compiled by Reati et al. (1996) suggests that the genera *Navicul*a and *Nitzschia* are the most common and numerous.

Sedimentary Organic Matter

Results

Values of TOC range from 0.0 to 3.5 wt%, with a mean of 2.1 wt% at nearshore sampling sites (see Table 2). Farther offshore, the concentration of TOC is largely similar, with a range from 0.0 to 4.6 wt% and a mean of 2.9 wt%. The richest concentration of TOC occurs in the western profundal EOD, whereas the sediments of the paleodelta are TOC poor (Fig. 4F). The range of TON values across the sample grid is from 0.0 to 0.90 wt%, with little difference between the sample value means of nearshore and offshore sites (0.36 versus 0.44 wt%). Contours of TON data (not shown) are broadly similar to TOC, and a cross-plot of wt% TOC versus TON exhibits relatively broad scatter (Fig. 5A). C/N means are consistent throughout the lake (8.3 versus 8.5 at nearshore and offshore sites, respectively); C/N rarely exceeds 9, and the highest values occur in the eastern profundal EOD.

Surface sediments at LMC exhibit a mean $\delta^{13}C_{OM}$ of –21.0‰ and a mean $\delta^{15}N$ of 5.0‰. The range of carbon isotope values is –23.5‰ to –19.8‰, with a slight shift toward more positive

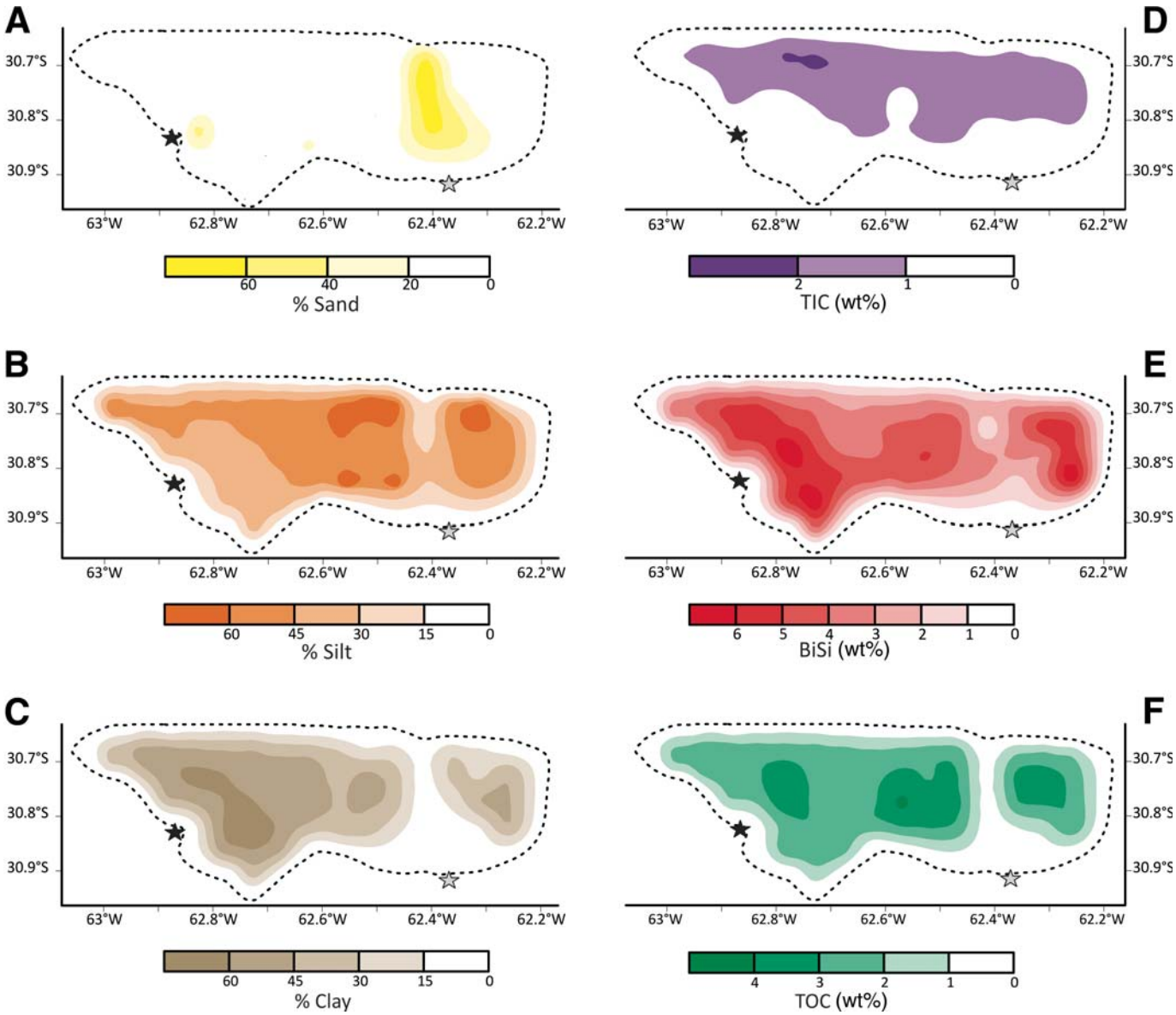

Figure 4. Contour maps of sedimentary components of Laguna Mar Chiquita (LMC) surface samples. Note the potential for unreliable data along the margins of the maps, where values are interpolated between sample points and the zero contour. A black star marks the mouth of the Río Primero, and a gray star marks the mouth of the Río Segundo Viejo. (A) Percent-sand contour map. The elongate sand wedge, coupled with shallow bathymetry, suggests the presence of an ancient deltaic environment of deposition (EOD). (B) Percent-silt contour map. The elevated concentration of silt on the western margin of the sample grid may reflect Campo Maare Formation dune sediments. (C) Percent-clay contour map. High clay concentration occurs in the western profundal EOD, interpreted to reflect suspension settling processes. (D) Weight percent total inorganic carbon (TIC) contour map. Authigenic calcite is common offshore, whereas ostracodes, gastropods, and foraminifera are found in nearshore samples. (E) Weight percent biogenic silica (BiSi) contour map. Diatoms appear to be the dominant source of biogenic silica in the lake (Reati et al., 1996), and contours suggest high productivity in profundal EODs. (F) Weight percent total organic carbon (TOC) contour map. Amorphous and pelleted organic matter are common components of LMC sediments, and relatively high values are found in profundal EODs.

values in samples collected from water depths >6 m (Fig. 5B). The range of nitrogen isotope values is from 0.03‰ to 8.3‰, with offshore samples exhibiting higher variability (Fig. 5C).

Hydrogen index (HI) values range from 27 to 315 mg HC/g TOC at nearshore sampling sites, with a mean of 200 mg HC/g TOC (Fig. 6A). In deeper water, HI values range from 40 to 399 mg HC/g TOC, with a mean of 220 mg HC/g TOC. For most samples, oxygen index (OI) values exceeded 200 mg CO_2/g TOC. Most of these data plot within the Type II kerogen field on a modified Van Krevelen diagram, with a few Type III samples. Maximum temperature data verify that OM from LMC is immature (Fig. 6B). Most LMC sediments show fair to good potential

TABLE 2. LAGUNA MAR CHIQUITA SURFACE SAMPLE GEOCHEMICAL DATA

Sample	Depth (m)	TOC (%)	TIC (%)	BiSi (%)	TON (%)	C/N	$\delta^{13}C_{OM}$ (‰)	$\delta^{15}N$ (‰)	HI	OI	*T*max (°C)	S_1	S_2
MC 01	6.4	2.70	1.20	2.67	0.46	6.8	–21.19	5.20	185	282	415	0.83	4.10
MC 02	6.8	2.85	0.73	5.31	0.35	9.5	–21.64	8.25	197	221	420	0.47	3.93
MC 03	6.9	2.88	1.41	3.66	0.54	6.2	–20.24	4.63	281	284	420	1.65	5.53
MC 04	6.9	2.99	1.70	2.58	0.55	6.3	–20.42	4.00	297	274	412	1.66	6.21
MC 05	6.4	2.53	2.00	3.04	0.45	6.6	–20.31	5.22	256	286	416	1.13	4.76
MC 06	6.2	2.29	1.83	3.09	0.38	7.0	–20.97	6.21	157	270	421	0.45	2.83
MC 07	6.7	2.57	1.69	4.01	0.42	7.1	–20.49	5.24	194	300	406	0.84	3.57
MC 08	6.5	2.52	1.72	3.31	0.44	6.7	–20.05	5.08	175	308	412	0.65	3.62
MC 09	6.1	2.96	1.33	5.40	0.47	7.3	–19.98	5.23	314	211	416	1.08	7.13
MC 10	4.7	0.06	0.53	1.34	N.D.	N.D.	–22.17	N.D.	114	331	412	0.09	0.54
MC 11	5.4	1.88	0.68	5.46	0.34	6.5	–22.55	5.68	173	275	385*	0.48	2.34
MC 12	6.6	2.86	0.48	7.44	0.23	14.5	–21.67	7.44	199	184	418	0.47	4.36
MC 13	7.0	2.93	0.93	5.55	0.35	9.8	–21.22	5.31	194	198	418	0.74	4.44
MC 14	6.9	2.44	1.00	4.82	0.39	7.3	–21.25	6.40	189	206	412	0.48	3.75
MC 15	6.8	2.55	1.96	4.10	0.33	9.0	–20.92	5.90	191	236	419	0.84	3.77
MC 16	6.2	2.51	2.03	3.82	0.34	8.6	–20.32	5.37	234	244	420	0.71	4.32
MC 17	6.3	2.62	2.33	3.86	0.42	7.3	–20.53	5.66	218	245	413	1.28	4.56
MC 18	6.4	3.47	1.49	4.68	0.55	7.4	–20.40	N.D.	224	208	413	1.16	5.28
MC 19	6.7	4.45	0.28	7.75	0.36	14.4	–21.63	7.70	207	191	414	0.48	4.29
MC 20	6.2	2.11	0.90	4.75	0.35	7.0	–22.09	6.19	181	216	414	0.39	3.02
MC 21	6.0	3.40	0.38	6.03	0.37	10.7	–21.69	5.69	198	214	406	0.64	3.98
MC 23	3.6	0.15	0.22	0.01	N.D.	N.D.	–22.31	N.D.	N.D.	N.D.	N.D.	N.D.	N.D.
MC 24	6.1	2.23	0.74	3.48	0.13	20.0	–20.68	4.55	273	255	412	1.16	4.94
MC 25	6.3	2.79	1.14	6.28	0.40	8.1	–21.36	5.28	221	276	396*	1.45	4.06
MC 26	5.8	2.61	1.42	5.00	0.38	8.0	–21.37	5.35	211	237	422	0.48	4.14
MC 27	5.2	2.90	1.40	5.19	0.40	8.5	–20.61	4.75	228	229	417	1.00	4.83
MC 28	5.9	2.55	1.37	4.80	0.37	8.0	–21.07	5.57	207	218	413	0.89	4.37
MC 29	5.6	2.57	1.43	5.26	0.38	7.9	–20.71	5.35	201	241	412	0.77	4.03
MC 30	3.9	2.89	0.47	3.99	0.36	9.4	–20.54	4.82	204	214	417	0.91	4.52
MC 31	3.8	2.94	1.74	4.45	0.45	7.6	–20.28	4.72	252	250	419	0.73	5.66
MC 32	3.0	2.54	1.26	3.47	0.33	9.0	–20.34	3.81	235	251	418	0.50	4.19
MC 33	4.1	2.83	0.67	5.17	0.34	9.7	–21.62	5.28	204	219	417	0.58	4.22
MC 34	5.8	N.D.	N.D.	4.49	N.D.	N.D.	N.D.	3.67	258	229	416	0.83	5.40
MC 34A	6.2	3.28	1.18	4.27	0.76	5.0	–20.01	3.61	399	186	392*	3.00	11.20
MC 35	6.5	4.60	0.01	4.41	0.90	6.0	–23.09	0.03	221	258	411	1.15	5.40
MC 36	6.6	3.20	1.10	4.22	0.53	7.0	–20.73	4.24	203	283	418	0.87	4.64
MC 37	6.2	2.46	1.38	2.99	0.34	8.4	–20.67	4.18	219	267	410	0.81	4.28
MC 38	6.3	2.82	1.28	3.92	0.47	7.0	–20.70	3.81	213	256	423	0.95	4.95
MC 39	6.6	2.58	1.75	3.82	0.42	7.2	N.D.	5.92	174	285	415	0.56	3.48
MC 40	6.6	3.05	1.26	5.28	0.50	7.1	N.D.	5.54	226	285	409	0.93	5.71
MC 41	6.1	3.24	1.56	4.11	0.50	7.6	–20.06	4.15	218	238	420	1.06	5.79
MC 42	5.6	2.94	1.38	3.46	0.41	8.4	–20.45	4.20	243	264	408	1.14	5.22
MC 43	6.5	3.82	1.12	4.00	N.D.	N.D.	–20.20	3.44	251	219	412	1.80	7.94
MC 44	6.6	3.40	1.20	4.92	0.68	5.8	–20.45	3.21	241	240	417	1.25	6.61
MC 45	6.4	2.98	1.35	3.21	0.39	8.9	–20.23	3.57	246	267	424	0.89	5.02
MC 47	4.2	0.28	0.46	3.11	N.D.	N.D.	–23.51	6.38	72	317	378*	0.10	0.28
MC 48	5.5	0.00	1.36	3.31	N.D.	N.D.	–22.12	N.D.	113	481	386*	0.08	0.15
MC 49	6.6	0.00	2.19	0.01	N.D.	N.D.	–21.27	N.D.	94	422	329*	0.03	0.06
MC 50	6.2	0.00	0.88	2.86	N.D.	N.D.	–22.94	N.D.	40	154	371*	0.03	0.11
MC 52	4.4	0.82	0.97	1.26	0.17	5.6	–22.28	7.54	126	268	415	0.20	0.62
MC 53	5.9	3.40	1.17	3.53	0.47	8.4	–20.31	4.17	315	179	412	2.49	8.40
MC 54	6.5	3.58	1.26	3.53	0.21	19.9	–20.28	1.78	317	184	421	2.05	9.16
MC 55	6.2	2.12	1.78	3.56	0.33	7.5	–21.17	6.05	179	248	420	0.61	2.98
MC 56	6.2	2.43	1.15	2.71	0.29	9.8	–20.44	4.29	202	238	416	0.82	3.70
MC 57	6.3	3.23	1.50	6.24	0.52	7.2	–20.77	4.91	263	205	420	1.47	6.94
MC 58	6.1	3.22	1.60	2.06	0.53	7.1	–19.78	4.59	286	275	417	1.62	6.49
MC 59	3.1	0.98	0.13	3.36	0.12	9.5	–20.81	6.66	27	148	398*	0.06	0.24
MC 62	4.9	3.49	0.87	8.45	0.53	7.7	–21.44	5.84	271	261	414	2.56	5.53
MC 63	5.8	2.75	1.74	5.50	0.46	7.0	–21.11	5.78	230	259	417	1.16	4.35
MC 64	6.1	2.69	1.45	5.59	0.41	7.7	–21.35	5.85	218	228	417	0.89	4.19
MC 65	6.0	2.52	0.76	3.58	0.32	9.2	–20.64	3.34	311	232	420	1.26	5.57

Note: TOC—total organic carbon; TIC—total inorganic carbon; BiSi—biogenic silica; TON—total organic nitrogen; C/N—ratio of carbon to nitrogen; HI—hydrogen index (mg HC/gm TOC); OI—oxygen index (mg CO_2/gm TOC); *T*max—temperature of peak S_2 (°C; values marked with asterisk may be unreliable due to a poorly resolved S_2 peak): S_1, S_2 (free and generatable hydrocarbons, respectively, in mg HC/gm sediment). Note that TON and C/N values have been corrected for contributions from inorganic nitrogen. N.D.—no data.

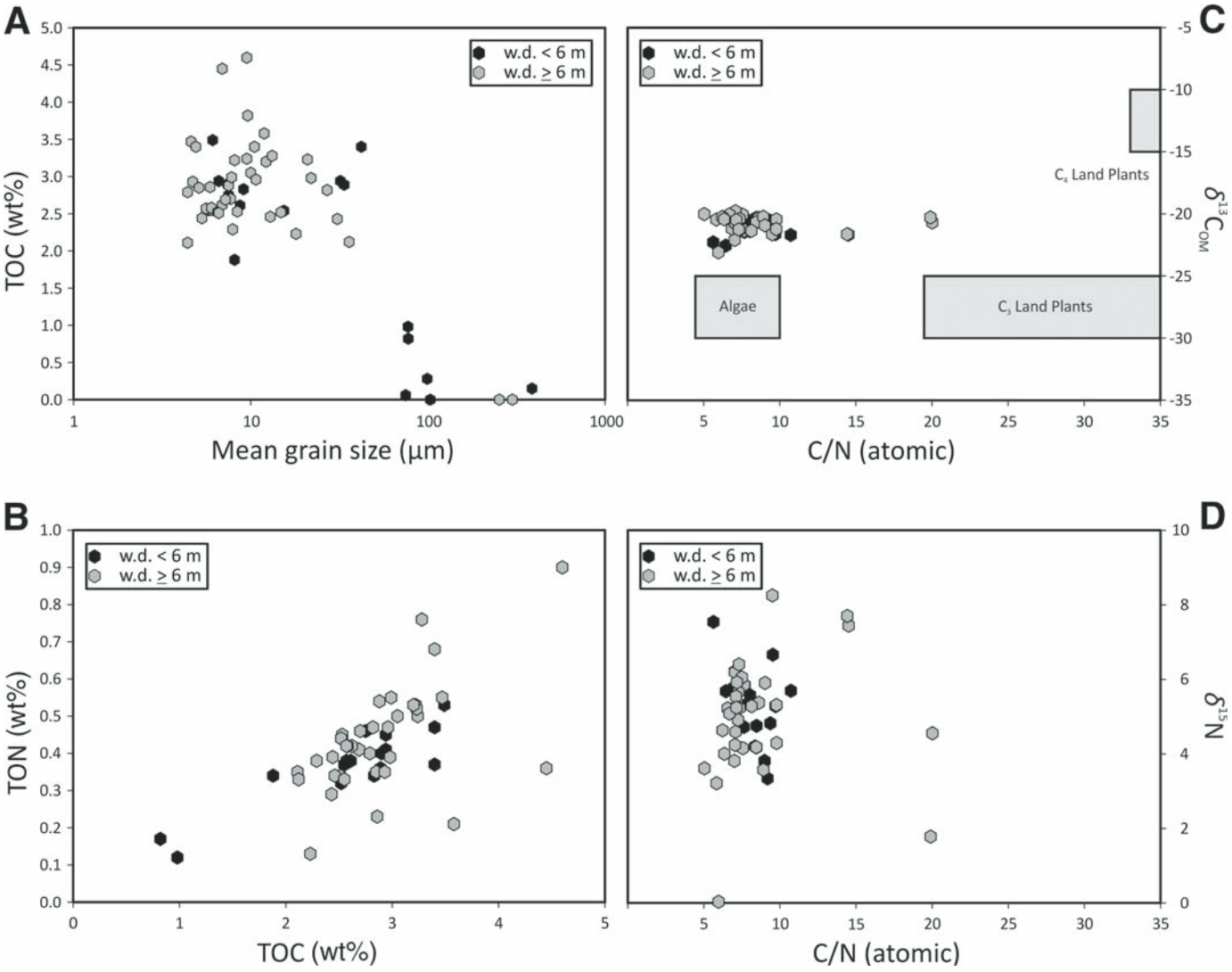

Figure 5. (A) Cross-plot of total organic carbon (TOC; wt%) versus mean terrigenous particle size (µm). All nearshore and offshore samples that are <50 µm exhibit petroleum source rock potential (TOC > 2.0 wt%). (B) Cross-plot of total organic carbon (TOC; wt%) versus total organic nitrogen (TON; wt%) (w.d.—water depth). Note that TON values have been corrected for contributions of inorganic nitrogen, and that these data are not available for all of the samples. Oxidation of organic matter (OM) in this low-accommodation lake basin may be responsible for the scatter in TON. (C) Cross-plot of carbon stable isotope (‰) versus ratio of carbon to nitrogen (C/N). Low C/N values indicate a predominantly algal source for OM. Piovano et al. (2002) reported that the effects of evaporation and ^{12}C-rich river water control the carbon isotopic composition of OM. The enriched $\delta^{13}C_{OM}$ values from our study are consistent with these findings. (D) Cross-plot of nitrogen stable isotopes (‰) versus ratio of carbon to nitrogen. The $\delta^{15}N$ data are consistent with values associated with nitrate and ammonium assimilation by algae, with a possible influence of agricultural runoff from the Laguna Mar Chiquita watershed.

as hydrocarbon source rocks, based on a cross-plot of total generation potential ($S_1 + S_2$; free and generatable hydrocarbons, respectively) versus TOC (Fig. 6C).

Interpretations

A contrast exists between nearshore and offshore TOC concentration (Fig. 4F), and the data make clear that OM richness is strongly linked with EOD during the current lake-level highstand at LMC. Figure 5D illustrates the link between TOC and mean detrital particle size. We interpret mean particle size to reflect gross depositional processes and environmental energy, as larger mean particle sizes require more energetic conditions for transport and deposition. This cross-plot shows that sediments with a mean particle size <~50 µm (coarse silt) contain ≥2.0 wt% TOC for all water depths. In contrast, samples with a mean particle size >50 µm contain low TOC and were recovered in specific depositional settings, such as the paleodelta and western lake margin. We interpret that matrix dilution by coarse siliciclastic detritus had an important impact on OM richness in these environments. This interpretation is supported by the relationship

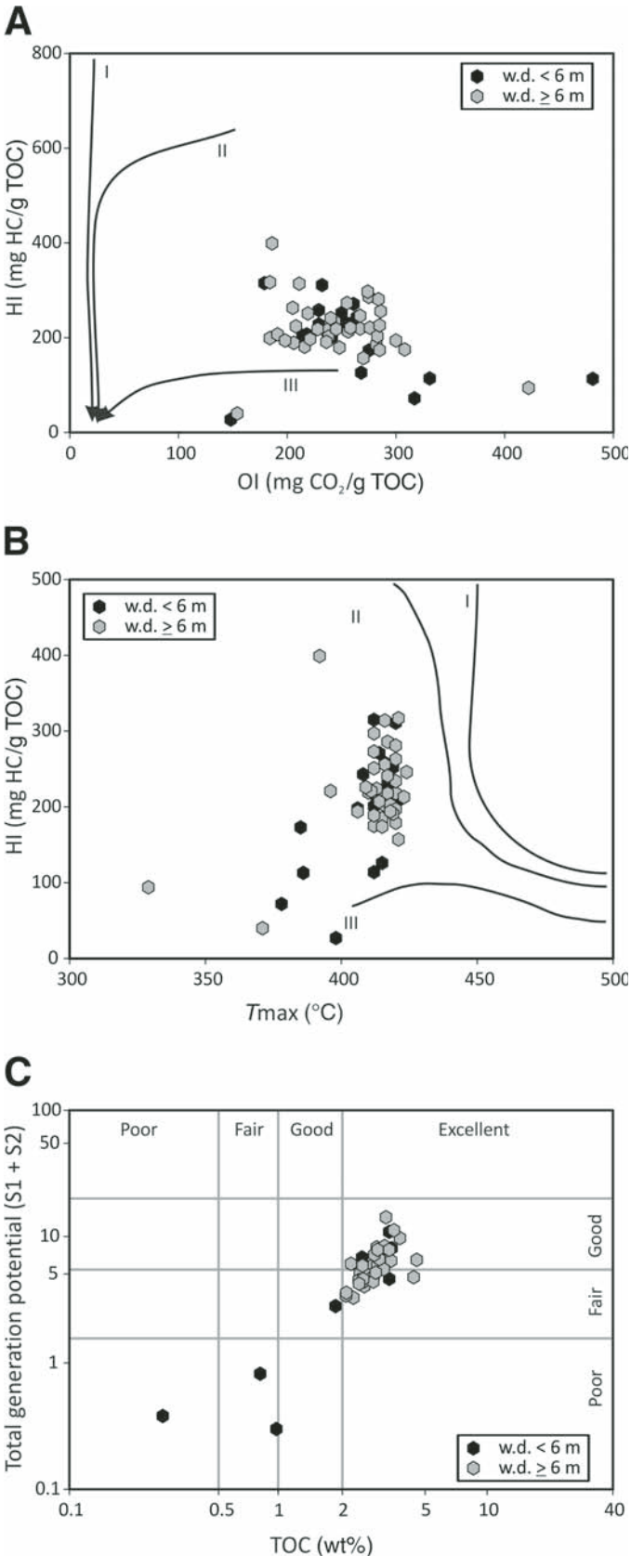

between particle size and water depth (Fig. 2D). Other processes may also limit the accumulation of OM along the paleodelta and western lake margin. For example, the shoal formed by deltaic sediments may lead to the development of contour currents and winnowing of fine-grained sediment during lake-level highstands (e.g., Johnson and Ng'ang'a, 1990). These accumulations are likewise subject to subaerial exposure and erosion during lowstands (e.g., McGlue et al., 2006). We interpret that wave action on the western LMC margin most likely limits the accumulation of fine-grained sediment to thin veneers on the submerged dune field, leading to a low ratio of OM to siliciclastic sediment. Oxidation and reworking of OM is common in these types of high-energy environments, further limiting TOC concentration.

We attribute the relatively broad scatter pattern in wt% TOC versus TON (Fig. 5A) to variable N preservation among LMC's depositional environments. C/N values are commonly used to place constraints on the provenance of OM (Meyers and Terranes, 2001). The relatively low C/N values observed in this study suggest that the origin of sedimentary OM is linked with aquatic algae, consistent with the findings of Piovano et al. (2004) and Varandas da Silva et al. (2008). Modern LMC sediments also contain inorganic N, which we interpret to be related to clay mineralogy (Talbot, 2001). Ammonium released from soil OM during weathering is known to adsorb to illite interlayers, and this clay is abundant in LMC surface sediments (Fig. 2C). It is plausible that higher soil weathering and erosion accompanying the lake-level rise that began in the 1970s may be responsible for this aspect of the modern sediment geochemistry.

Generally, the carbon isotope composition of lacustrine sedimentary OM is controlled by the dissolved inorganic carbon pool of the lake water and by organic fractionation. A detailed study of $\delta^{13}C_{OM}$ from short cores and modern plankton was presented in Piovano et al. (2004). The mean basin-wide surface sediment $\delta^{13}C_{OM}$ from our study (–21.02‰) is very close to that of plankton reported in Piovano et al. (2004) (–20.9‰ and –20.1‰ for winter and summer samples, respectively). Piovano et al. (2004) concluded that during lake-level highstands, the combined effects of evaporation, which enriches lake water in ^{13}C through kinetic effects, and inflowing ^{12}C-rich riverine water control the isotopic composition of OM. By contrast, when LMC is at lowstand, evaporation is at a maximum and lake waters are highly alkaline,

Figure 6. Rock-Eval pyrolysis data for Laguna Mar Chiquita (LMC) (w.d.—water depth). (A) Modified Van Krevelen diagram. Although most samples plot within the Type II kerogen field, it is likely that these values reflect degradation of lacustrine algal organic matter (OM); the strong likelihood of oxidation is captured by the oxygen index (OI; HI—hydrogen index). (B) Cross-plot of HI (mg hydrocarbon, HC/g total organic carbon, TOC) versus the temperature of peak S_2 (*T*max, °C). The data show that OM from LMC is immature. (C) Cross-plot of total hydrocarbon generation potential ($S_1 + S_2$) versus total organic carbon (wt%). Most sediment samples show fair to good source rock potential, which attests to the efficacy of highstand primary productivity in this basin.

carbonate accumulation rates rise, and aquatic organisms mostly likely utilize HCO_3^- as a carbon source for photosynthesis, leading to more positive $\delta^{13}C_{OM}$ (Piovano et al., 2004).

The nitrogen isotope composition of lacustrine sedimentary OM is principally a function of the isotopic composition and concentration of bioavailable nitrogen (Talbot, 2001). In lakes, dissolved inorganic nitrogen typically takes the form of nitrate (dominant under oxidizing conditions) or ammonium (dominant under strong reducing conditions), and in rare instances dissolved N_2 can become important (Talbot, 2001). The range of $\delta^{15}N$ (Fig. 5C) at LMC is consistent with nitrate and ammonium assimilation by algae, which is not unusual for lakes in the subtropics that undergo seasonal mixing (e.g., Talbot and Johannessen, 1992). Notably, much of the land cover around the lake has been modified for agriculture. Nutrient loading associated with farming is known to have increased $\delta^{15}N$ values in other large lakes (Talbot, 2001 and references therein), but prehistoric records of $\delta^{15}N$ from LMC are not available.

Rock-Eval data suggest that with the exception of a few nearshore samples, most of LMC muds hold the potential for hydrocarbon generation ($S_1 + S_2 > 2.5$ mg HC/g sediment; after Katz, 1990). However, these values are subject to the uncertainties associated with the Rock-Eval method (e.g., potentially poor separation between the S_1 and S_2 peaks) for immature sediments (Peters, 1986). Given that modal C/N is <10, the low HI values are most consistent with a degraded algal source; this is not unusual for geologically young sediments from shallow polymictic lakes (e.g., McGlue et al., 2011). Oxygen index values (Fig. 6A) highlight the effects of diagenesis that most likely capture the oxidation of OM settling through the upper water column. Reworking of OM by waves in nearshore environments most likely contributes to elevated OI values, and the highest values are encountered in the paleodelta EOD. Farther offshore, the lake floor escapes significant reworking, as fine (millimeter scale) laminations were obvious in some of our samples, and limited oxygen most likely helps to preserve OM during early sedimentation. The hydrocarbon source potential implied by Rock-Eval data attest to productivity at LMC when lake levels are high, an inference supported by relatively high ^{210}Pb-derived organic accumulation rates for the past 35 yr (Piovano et al., 2002). There are no Rock-Eval data for LMC during lake-level lowstands.

DISCUSSION

Lacustrine Source Rocks: The LMC Analog

Conclusive stratigraphic evidence of large underfilled lakes exists for a number of thick-skinned forelands in the western United States, including the Green River, Uinta, Washakie, Sand Wash, and Piceance Creek Basins (Bradley and Eugster, 1969; Bohacs et al., 2000; Lawton, 2008). Although Cretaceous marine shales are the most typical source rocks in many Laramide petroleum systems, in some instances the low-maturity saline-lake strata of these basins have developed vast stores of oil (Dubiel, 2003; Johnson et al., 2011). For example, Carroll and Bohacs (2001) noted that the sublittoral muds of the Eocene Wilkins Peak Member are characterized by Type I kerogen and high mean TOC values (~7.3 wt%), revealing excellent source-rock potential for these saline-lake sediments. We consider LMC to be a partial analog to the early Cenozoic saline-lake phases of these Laramide forelands, due to similarities in tectonic setting, semiarid climate, closed hydrology, and the impact of large-scale drainage evolution on sedimentation in these basins (e.g., Smith et al., 2008; Davis et al., 2009). The extensive spatial coverage of our sample grid makes comparisons between modern LMC and ancient analogs feasible, and allows hypotheses on organic facies developed from outcrop and well data to be tested.

The model for organic facies evolution in underfilled lake basins developed by Carroll and Bohacs (2001) emphasized highstand deposition under hypersaline and often anoxic conditions, with minimal lateral variability in HI across depositional environments. Our results generally support this model, as the organic-rich muds that characterize profundal EODs began to accumulate following the 1970s transgression (Piovano et al., 2002). Relatively narrow ranges of $\delta^{13}C_{OM}$ and HI likewise characterize LMC profundal muds (Figs. 5B and 6A). The geochemistry of these muds suggests that elevated algal productivity influenced their development, which is consistent with C_{27} (dominant), C_{28}, and C_{29} sterols reported by Varandas da Silva et al. (2008). Productivity during highstands is likely also influenced by increased nutrient input associated with flooded lake margins and adjacent plains (e.g., Buchheim and Eugster, 1998). In contrast, carbonate muds with low TOC and significant contributions from C_4 vascular plants accumulated during low and intermediate lake levels from 1767 to 1975, apparently due to reduced productivity and algal diversity in a hypersaline water column (Piovano et al., 2004; Varandas da Silva et al., 2008). Taken together, these data indicate that the quality and quantity of OM at LMC is strongly influenced by lake level, which is similar to other large tectonic lakes affected by climate-driven lake-level fluctuations on 10^2–10^4 yr time scales (e.g., Huc et al., 1990; Katz, 1990, 2001).

Detrital particle size exhibits an inverse correlation with water depth at LMC, and muds with high TOC concentrations are typically characterized by <10 μm mean particle size (Figs. 2D and 5D). Abundant clay and fine silt particles in the profundal EOD may also assist in constraining interstitial oxygen, promoting better preservation of OM (Gray, 1981; McGlue et al., 2012). This pattern is consistent with the underfilled lake-basin organic sedimentation model of Carroll and Bohacs (2001). Bohacs et al. (2000) explained that siliciclastic dilution of organic-rich muds is uncommon in the depocenters of large underfilled lakes, as lake expansion during highstands floods basin margins and restricts transport of coarse detritus. Therefore, dilution at LMC should be most notable in the paleodelta and lake margin EODs, a prediction that is validated by our percent sand and percent silt contour maps (Figs. 4A, 4B).

Organic matter preservation is also critical to petroleum potential in underfilled lake basins. In basins with significant accommodation space, aggradational stacking of parasequences in restricted and often anoxic basin-center environments helps to preserve organic facies, even during lake-level lowstands; evidence suggests that this was the case for the Wilkins Peak Member (Bohacs et al., 2000; Carroll and Bohacs, 2001). Insights from geodynamic models suggest that the total stratal thickness of the LMC basin is on the order of several hundred meters (Dávila et al., 2010; Fig. 1C). Coupled with bathymetry data, this indicates relatively low accommodation space for LMC. Whereas stable water-column stratification and persistent seasonal anoxia was likely in the underfilled lakes of the Green River Formation, the LMC well-mixed water column and relatively shallow sublittoral maximum water depths are far less favorable for the development of organic facies. The bathymetry implies that oxidation of OM in the well-mixed water column is common at highstands (confirmed by OI values; Fig. 6A), as is subaerial exposure and erosion during lowstands. Although the lake is well mixed on an annual basis, sediments accumulating today do so under reducing conditions, which in concert with productivity levels may help explain deposition of muds with TOC > 2.0% (Fig. 4F). This is apparently due to sulfate-reducing bacteria, which at times may have been responsible for dysoxic conditions at the lake bottom (Piovano et al., 2002, and references therein).

Insights on Lacustrine Unconventional Resources

With the growing need for petroleum resources globally and advances in hydraulic fracturing, it is instructive to consider the potential of lacustrine mudrocks as unconventional gas reservoirs using the LMC analog. To date, most prolific shale-gas plays have had their origins in foreland basins and marine source rocks, such as the Barnett Shale (Fort Worth Basin, USA; Pollastro et al., 2007). In general, the important mechanisms of natural gas storage in fine-grained reservoirs are: (1) OM richness, type, and maturity; (2) mineral composition; (3) porosity characteristics; and (4) moisture content (e.g., Ross and Bustin, 2009). The adsorption experiments of Zhang et al. (2012) revealed that the methane capacity of shales is enhanced by kerogen type (Type III > Type II > Type I) and increasing TOC concentration. Given these results, the profundal muds of LMC (mean offshore TOC = 2.9 wt%) appear to hold modest potential for gas storage. Furthermore, XRD results indicate that on average, the muds of LMC contain ~33% clay minerals, 10% calcite, 7% quartz, and 4.5% halite plus gypsum, with the balance made up of feldspars, altered volcanic glass, and amorphous material (OM and diatoms). Ross and Bustin (2007) showed that although quartz and carbonate have low gas-sorption capacities (due to low internal surface areas), the internal structure of illite has among the highest gas-sorption capacity of all the clays (to ~3 cm^3/g at 30 °C and 7 MPa). Even though moisture content can reduce the efficacy of gas sorption in clay (Zhang et al., 2012), the abundance of illite in the clay-mineral fraction of LMC sediments is potentially favorable for unconventional gas storage. Higher risk is usually assigned to lacustrine shales for unconventional gas based on *a priori* assumptions regarding total clay content (Kuuskraa et al., 2011). The presence of diatoms, quartz, and carbonate also contribute to the brittleness of LMC organic facies, which are known to be critical to successful stimulation and gas flow (e.g., Jarvie et al., 2007). The coarser grained facies identified in this study could also provide higher matrix porosity for unconventional gas plays, as fluctuations in lake levels could generate stacked sequences of fine-grained OM-rich sediments interbedded with these coarser-grained reservoir rocks.

Thick-Skinned versus Thin-Skinned Lacustrine Foreland Petroleum Systems

Lakes form in forelands when climate conditions and rates of sediment supply favor the preservation of accommodation space (e.g., Carroll and Bohacs, 1999). Sladen (1994) indicated that lakes form in compressional basins during intermediate stages of evolution, which nominally involved mountain belt growth and maximum flexural subsidence. Similar to the model proposed for rift basins by Lambiase (1990), thick packages of lacustrine sediment were expected to occur between early synorogenic and late postorogenic alluvial sequences, when foredeep subsidence outpaced sedimentation (Sladen, 1994). Because of diachronous thrusting and lateral movement of the flexural profile, this model predicted migrating lake depocenters and offset vertical stacking of muds in these basins, similar to the fluvial-lacustrine facies model discussed by Beck et al. (1988). The majority of flexural basins with prolific lacustrine hydrocarbon systems cited by Sladen (1994) occurred in thick-skinned foreland basins, similar to LMC. This is because large and stable lake systems rarely form in thin-skinned foreland basins, most likely because the rates of sediment infilling are strongly influenced by effective precipitation, and outpace tectonic subsidence. The modern central Andean foreland provides a striking example of this overfilled condition, as transverse fluvial megafans constitute the main foredeep depositional environments and large lakes are absent (e.g., Horton and DeCelles, 1997; Latrubesse et al., 2012; Cohen et al., 2014). In addition to climate, watershed geology exerts another important control on lake formation. Most thin-skinned thrust belts consist of highly erodable marine-siliciclastic lithologies, within which bedload-dominant distributary drainages commonly form (Horton and DeCelles, 2001). Consequently, the strata of large lakes have usually been encountered where conditions were both arid and the watershed consisted of carbonate lithologies, conditions that favor rivers with low ratios of bedload to dissolved load (e.g., Lakes Peterson and Draney of the Sevier foreland; Zaleha, 2006). Topographic closure and lake formation is much more likely in thick-skinned systems because of the dominance of crystalline basement rocks in their watersheds, which reduce rates of basin infilling and help maintain a viable foredeep (e.g., Carroll et al., 2006).

In many cases, hydrocarbons associated with retroarc thrust belts and thin-skinned forelands are produced by ductile

preorogenic marine source rocks that also serve as detachment surfaces for individual thrust sheets (Nemčok et al., 2005). As a result, the usual targets for many exploration wells in this tectonic setting are hanging-wall traps of the medial thrust belt (e.g., Dunn et al., 1995). In early foreland exploration models, late-stage continental strata with gas-prone Type III OM were expected proximal to the thrust belt, but the spatiotemporal evolution of these deposits was difficult to predict. Conceptual models of thin-skinned foreland basin stratigraphy have evolved significantly over the past several decades (Dickinson, 1974; Beaumont, 1981; Heller et al., 1988; Flemings and Jordan, 1989; Jordan, 1995; DeCelles and Giles, 1996). It is now generally accepted that these foreland basins may consist of several discrete depozones (e.g., wedgetop, foredeep, forebulge, and back bulge) that form under different kinematic and subsidence conditions (DeCelles, 2011). The depozones may receive sediment from a variety of sources in addition to the adjacent fold-thrust belt, such as the craton or the forebulge (e.g., DeCelles, 2004). Flexure derived from fold-thrust belt growth is the dominant mechanism of subsidence, but additional loads, such as those associated with a viscous coupling (via a mantle wedge) between the subducting oceanic plate and the overriding continental plate, may be important for fully realized forebulge and back-bulge depozones, especially in retroarc systems (DeCelles and Giles, 1996). An important aspect of foreland basin geodynamics is the lateral migration of the flexural profile with continued shortening, which serves to stack the strata of individual depozones in a predictable vertical succession (Fig. 7; DeCelles, 2011). In the context of lacustrine hydrocarbon systems, it is in this concept where a load imparted by a viscous coupling (so-called dynamic subsidence) can become especially important, since large lakes are so rare in the foredeep depozone. Back-bulge preservation may be critical to the accumulation of organic-rich strata and source development. For example, the hydrocarbon-producing black shales of the Eocene Bhainskati

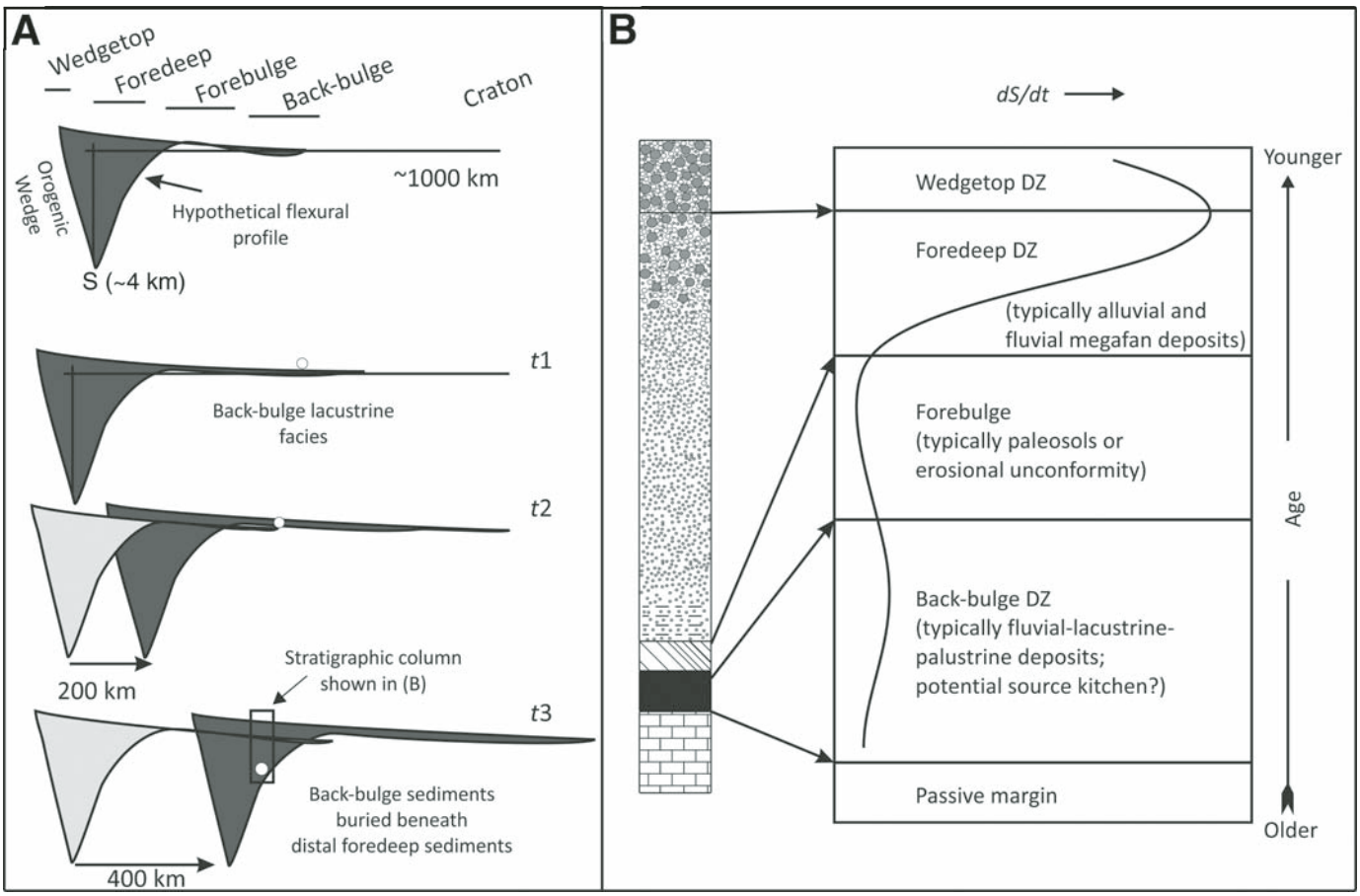

Figure 7. Model of lacustrine source rocks in the context of a thin-skinned foreland basin system. (A) Exaggerated cross section of a notional foreland basin system modified after DeCelles and Giles (1996) and DeCelles et al. (1998). Contraction in the orogen and migration of the flexural basin toward the craton stacks wedgetop, foredeep, forebulge, and back-bulge depozones (DZ), as shown in B. Time increases moving downward. *t*1—time 1 (initial basin development and subsidence). *t*2—time 2 (migration of flexural profile ~200 km). *t*3—time 3 (migration of flexural profile ~400 km); S—subsidence. (B) Foreland basin stratigraphy and *dS/dt* (change in subsidence with time, *t*). Preservation of the back-bulge depozones may be key for lacustrine source development, which follows vertical juxtaposition of fine-grained, organic-rich lacustrine and wetland deposits with foredeep megafan sandstones.

Formation of Nepal and its equivalents in India and Pakistan formed in a restricted marine back-bulge basin associated with the Himalayan foreland (Rahman and Kinghorn, 1995; DeCelles et al., 1998; Singh et al., 2000). In the modern Andean foreland, the wetlands of the Pantanal (Brazil) and humid Chaco (Bolivia, Argentina, and Paraguay; $>1 \times 10^6$ km^2 total) actively accumulate peat and OM in thousands of floodplain lakes and swamps (Iriondo, 2004; McGlue et al., 2011). The modern central Andean system is a useful analog for play-element prediction in ancient nonmarine forelands with preserved back-bulge depozones, because these deposits are stacked beneath the forebulge and potential reservoir sands of the foredeep (Fig. 7).

SUMMARY

1. Laguna Mar Chiquita, Argentina's largest saline lake, occupies a thick-skinned foreland basin in the Sierras Pampeanas. The tectonic origins of LMC are analogous to one of the most prolific oil shale–producing ancient lake systems in the world, the Wilkins Peak Member of the Eocene Green River Formation (western United States).

2. Although a simple historical model for sedimentation exists for LMC (Piovano et al., 2002), very little information is available that relates the influence of depositional environment on organic facies development, which is known to be critical for lacustrine hydrocarbon systems (e.g., Huc et al., 1990). We collected a grid of lake-floor sediment samples to investigate this relationship, using a variety of analyses to quantify fabric, mineralogy, and OM composition.

3. Particle-size trends and bathymetric data reveal that LMC consists of two profundal (western, primary; eastern, secondary), a paleodelta, and lake margin EODs. Our results indicate that organic-rich muds (average TOC = 2.9 wt%) are most common in the profundal environments, where fine particle sizes deposited by suspension settling prevail. In contrast, sediments of the margin and paleodelta environments consist of abundant coarse-grained terrigenous material and minor OM. Accumulations of OM are constrained in all environments by water-column oxidation and the lake's mixing state, and by wave action at shallow water depths.

4. Elemental, stable isotope, and Rock-Eval analyses indicate dominantly algal OM in the profundal EODs with minimal lateral variability; these muds have modest petroleum source potential. However, LMC lacks significant accommodation space, limiting aggradational stacking of organic facies during highstands and exacerbating OM preservation problems during lake-level lowstands.

5. We present conceptual models for continental hydrocarbon systems in thick-skinned and thin-skinned foreland basins. Foredeep lake strata are key source rock and potential unconventional targets in thick-skinned forelands, whereas back-bulge lake and wetland strata may be important in thin-skinned settings, where fold-thrust belt evolution and migration of the flexural profile stacks these deposits beneath potential distal foredeep reservoirs.

ACKNOWLEDGMENTS

The Petroleum Research Fund (45910-AC8), ExxonMobil, and the University of Arizona COSA Program provided funding for this research. E. Piovano provided an initial introduction to Laguna Mar Chiquita. We are grateful to H. Zani, P. Michelutti, and the staff of the Reserva Natural Mar Chiquita for assistance with data collection. We thank K. McDougall-Reid (U.S. Geological Survey, USGS) for the foraminifera identification, and M. Dreier (USGS) for producing the carbon isotope data. We also thank L. Peyton and R. Bottjer for their helpful discussions and constructive comments, and N. Fishman, C. Gans, P. Buchheim, A. Carroll, D. Ferderer, and K. Lucey for detailed reviews that improved the manuscript. Any use of trade, product, or firm names is for descriptive purposes only and does not imply endorsement by the U.S. government.

REFERENCES CITED

Beaumont, C., 1981, Foreland basins: Royal Astronomical Society Geophysical Journal, v. 65, p. 291–329, doi:10.1111/j.1365-246X.1981.tb02715.x.

Beck, R.A., Vondra, C.F., Filkins, J.E., and Olander, J.D., 1988, Syntectonic sedimentation and Laramide basement thrusting, Cordilleran foreland: Timing of deformation, *in* Schmidt, C.J., and Perry, W.J., Jr., eds., Interaction of the Rocky Mountain Foreland and the Cordilleran Thrust Belt: Geological Society of America Memoir 171, p. 465–487, doi:10.1130/MEM171-p465.

Bohacs, K.M., Carroll, A.R., Neal, J.E., and Mankeiwicz, P.J., 2000, Lake-basin type, source potential, and hydrocarbon character: An integrated sequence-stratigraphic- geochemical framework, *in* Gierlowski-Kordesch, E.H., and Kelts, K.R., eds., Lake Basins Through Space and Time: American Association of Petroleum Geologists Studies in Geology 46, p. 3–33.

Bradley, W.H., and Eugster, H.P., 1969, Geochemistry and Paleolimnology of the Trona Deposits and Associated Authigenic Minerals in the Green River Formation of Wyoming: U.S. Geological Survey Professional Paper 496-B, 71 p.

Brownfield, M.E., Mercier, T.J., Johnson, R.C., and Self, J.G., 2010, Nahcolite resources in the Green River Formation, Piceance Basin, Colorado, *in* U.S. Geological Survey Oil Shale Assessment Team, eds., Oil Shale Assessment of the Piceance Basin, Colorado: U.S. Geological Survey Digital Data Series 69–Y, 57 p.

Buchheim, H.P., and Eugster, H.P., 1998, Eocene fossil lake: The Green River Formation of Fossil Basin, southwestern Wyoming, *in* Pitman, J.K., and Carroll, A.R., eds., Modern and Ancient Lake Systems: Utah Geological Association Guidebook 26, p. 191–207.

Cahill, T., and Isacks, B., 1992, Seismicity and shape of the subducted Nazca plate: Journal of Geophysical Research, v. 97, p. 17,503–17,529, doi:10.1029/92JB00493.

Cann, J.H., and De Deckker, P., 1981, Fossil Quaternary and living foraminifera from athalassic (non-marine) saline lakes, southern Australia: Journal of Paleontology, v. 55, p. 660–670.

Carroll, A.R., and Bohacs, K.M., 1999, Stratigraphic classification of ancient lakes: Balancing tectonic and climatic controls: Geology, v. 27, p. 99–102, doi:10.1130/0091-7613(1999)027<0099:SCOALB>2.3.CO;2.

Carroll, A.R., and Bohacs, K.M., 2001, Lake-type controls on petroleum source rock potential in nonmarine basins: American Association of Petroleum Geologists Bulletin, v. 85, p. 1033–1053.

Carroll, A.R., Chetel, L., and Smith, M.E., 2006, Feast to famine: Sediment supply control on Laramide basin fill: Geology, v. 34, p. 197–200, doi:10.1130/G22148.1.

Cohen, A., McGlue, M.M., Ellis, G.S., Zani, H., Swarzenski, P.W., Assine, M.L., and Silva, A., 2014, Lake formation, characteristics, and evolution in retroarc deposystems: A synthesis of the modern Andean orogen and its associated basins, *in* DeCelles, P.G., Ducea, M.N., Carrapa, B., and Kapp, P.A., eds., Geodynamics of a Cordilleran Orogenic System: The Central Andes of Argentina and Northern Chile: Geological Society of America Memoir 212, doi:10.1130/2015.1212(16).

Dargám, M., 1994, Geochemistry of waters and brines from Salinas Grandes basin, Cordoba, Argentina. I. Geomorphology and hydrochemical characteristics: International Journal of Salt Lake Research, v. 3, p. 137–158, doi:10.1007/BF01990491.

Dávila, F.M., Lithgow-Bertelloni, C., and Giménez, M., 2010, Tectonic and dynamic controls on the topography and subsidence of the Argentine Pampas: The role of the flat slab: Earth and Planetary Science Letters, v. 295, p. 187–194, doi:10.1016/j.epsl.2010.03.039.

Davis, S.J., Mulch, A., Carroll, A.R., Horton, T.W., and Chamberlain, C.P., 2009, Paleogene landscape evolution of the central North American Cordillera: Developing topography and hydrology in the Laramide foreland: Geological Society of America Bulletin, v. 121, p. 100–116, doi:10.1130/B26308.1.

DeCelles, P.G., 2004, Late Jurassic to Eocene evolution of the Cordilleran thrust belt and foreland basin system, western U.S.A: American Journal of Science, v. 304, p. 105–168, doi:10.2475/ajs.304.2.105.

DeCelles, P.G., 2011, Foreland basin systems revisited: Variations in response to tectonic settings, *in* Busby, C., and Azor, A., eds., Tectonics of Sedimentary Basins: Recent Advances: Chichester, UK, John Wiley & Sons, p. 405–426, doi:10.1002/9781444347166.ch20.

DeCelles, P.G., and Giles, K.A., 1996, Foreland basin systems: Basin Research, v. 8, p. 105–123, doi:10.1046/j.1365-2117.1996.01491.x.

DeCelles, P.G., Gehrels, G.E., Quade, J., and Ojha, T.P., 1998, Eocene–early Miocene foreland basin development and the history of Himalayan thrusting, western and central Nepal: Tectonics, v. 17, p. 741–765, doi:10.1029/98TC02598.

Dickinson, W.R., 1974, Plate tectonics and sedimentation, *in* Dickinson, W.R., ed., Tectonics and Sedimentation: Society of Economic Paleontologists and Mineralogists Special Publication 22, p. 1–27, doi:10.2110/pec.74.22.0001.

Dubiel, R.F., 2003, Geology, depositional models, and oil and gas assessment of the Green River total petroleum system, Uinta-Piceance Province, eastern Utah, and western Colorado, *in* USGS Uinta-Piceance Assessment Team, compilers, Petroleum systems and geologic assessment of oil and gas the Uinta-Piceance Province, Utah and Colorado: U.S. Geological Survey Digital Data Series DDS-69-B, 45 p. [CD-ROM].

Dunn, J.F., Hartshorn, K.G., and Hartshorn, P.W., 1995, Structural styles and hydrocarbon potential of the sub-Andean thrust belt in southern Bolivia, *in* Tankard, A.J., Suarez-Soruco, R., and Welsink, H.J., eds., Petroleum Basins of South America: American Association of Petroleum Geologists Memoir 62, p. 523–543.

Dyni, J.R., 1996, Sodium carbonate resources of the Green River Formation: U.S. Geological Survey Open-File Report 96–729, 39 p.

Eberl, D.D., 2003, User guide to RockJock—A program for determining quantitative mineralogy from X-ray diffraction data: U.S. Geological Survey Open File Report 03–78, 48 p.

Eugster, H., and Hardie, L.A., 1975, Sedimentation in an ancient playa-lake complex: The Wilkins Peak Member of the Green River Formation of Wyoming: Geological Society of America Bulletin, v. 86, p. 319–334, doi:10.1130/0016-7606(1975)86<319:SIAAPC>2.0.CO;2.

Flemings, P.B., and Jordan, T.E., 1989, A synthetic stratigraphic model of foreland basin development: Journal of Geophysical Research, v. 94, p. 3851–3866, doi:10.1029/JB094iB04p03851.

Folk, R.L., 1980, Petrology of Sedimentary Rocks: Austin, Texas, Hemphill Publishing, 182 p.

Furquim, S.A.C., Graham, R.C., Barbiero, L., Queiroz Neto, J.P., and Vallès, V., 2008, Mineralogy and genesis of smectites in an alkaline-saline environment of Pantanal wetland, Brazil: Clays and Clay Minerals, v. 56, p. 579–595, doi:10.1346/CCMN.2008.0560511.

Gans, C.R., Beck, S.L., Zandt, G., Gilbert, H., Alvarado, P., Anderson, M., and Linkimer, L., 2011, Continental and oceanic crustal structure of the Pampean flat slab region, western Argentina, using receiver function analysis: New high-resolution results: Geophysical Journal International, v. 186, p. 45–58, doi:10.1111/j.1365-246X.2011.05023.x.

Genta, J.L., Perez Iribarren, G., and Mechoso, C., 1998, A recent increasing trend in the streamflow of rivers in southeastern South America: Journal of Climate, v. 11, p. 2858–2862, doi:10.1175/1520-0442(1998)011<2858:ARITIT>2.0.CO;2.

Gray, J.S., 1981, The Ecology of Marine Sediments: An Introduction to the Structure and Function of Benthic Communities: Cambridge, UK, Cambridge University Press, 185 p.

Heller, P.L., Angevine, C.L., Winslow, N.S., and Paola, C., 1988, 2-phase stratigraphic model of foreland-basin sequences: Geology, v. 16, p. 501–504, doi:10.1130/0091-7613(1988)016<0501:TPSMOF>2.3.CO;2.

Horton, B.K., 2011, Cenozoic evolution of hinterland basins in the Andes and Tibet, *in* Busby, C., and Azor, A., eds., Tectonics of Sedimentary Basins: Recent Advances: Chichester, UK, John Wiley & Sons, p. 427–444, doi:10.1002/9781444347166.ch21.

Horton, B.K., and DeCelles, P.G., 1997, The modern foreland basin system adjacent to the central Andes: Geology, v. 25, p. 895–898, doi:10.1130/0091-7613(1997)025<0895:TMFBSA>2.3.CO;2.

Horton, B.K., and DeCelles, P.G., 2001, Modern and ancient fluvial megafans in the foreland basin system of the central Andes, southern Bolivia: Implications for drainage network evolution in fold-thrust belts: Basin Research, v. 13, p. 43–63, doi:10.1046/j.1365-2117.2001.00137.x.

Huc, A.Y., LeFournier, J., Vandenbroucke, M., and Bessereau, G., 1990, Northern Lake Tanganyika; an example of organic sedimentation in an anoxic rift lake, *in* Katz, B.J., ed., Lacustrine Basin Exploration: Case Studies and Modern Analogs: American Association of Petroleum Geologists Memoir 50, p. 169–185.

Iriondo, M., 2004, Large wetlands of South America: A model for Quaternary humid environments: Quaternary International, v. 114, p. 3–9, doi:10.1016/S1040-6182(03)00037-5.

Jarvie, D.M., Hill, R.J., Ruble, T.E., and Pollastro, R.M., 2007, Unconventional shale-gas systems: The Mississippian Barnett Shale of north-central Texas as one model for thermogenic shale-gas assessment: American Association of Petroleum Geologists Bulletin, v. 91, p. 475–499, doi:10.1306/12190606068.

Johnson, R.C., Mercier, T.J., and Brownfield, M.E., 2011, Assessment of in-place oil shale resources of the Green River Formation, Greater Green River Basin in Wyoming, Colorado, and Utah: U.S. Geological Survey Fact Sheet 2011-3063, 4 p.

Johnson, T.C., and Ng'ang'a, P., 1990, Reflections on a rift lake, *in* Katz, B.J., ed., Lacustrine Basin Exploration: Case Studies and Modern Analogs: American Association of Petroleum Geologists Memoir 50, p. 113–135.

Jordan, T.E., 1995, Retroarc foreland and related basins, *in* Busby, C.J., and Ingersoll, R.V., eds., Tectonics of Sedimentary Basins: Cambridge, UK, Blackwell Science, p. 331–362.

Jordan, T.E., and Allmendinger, R.W., 1986, The Sierras Pampeanas of Argentina: A modern analogue of Rocky Mountain foreland deformation: American Journal of Science, v. 286, p. 737–764, doi:10.2475/ajs.286.10.737.

Katz, B.J., 1990, Controls on distribution of lacustrine source rocks through time and space, *in* Katz, B.J., ed., Lacustrine Basin Exploration: Case Studies and Modern Analogs: American Association of Petroleum Geologists Memoir 50, p. 61–76.

Katz, B.J., 2001, Lacustrine basin hydrocarbon exploration—Current thoughts: Journal of Paleolimnology, v. 26, p. 161–179, doi:10.1023/A:1011173805661.

Kay, S.M., and Abbruzzi, J.M., 1996, Magmatic evidence for Neogene lithospheric evolution of the central Andean "flat-slab" between 30°S and 32°S: Tectonophysics, v. 259, p. 15–28, doi:10.1016/0040-1951(96)00032-7.

Kröhling, D.M., and Iriondo, M., 1999, Upper Quaternary palaeoclimates of the Mar Chiquita area, North Pampa, Argentina: Quaternary International, v. 57–58, p. 149–163, doi:10.1016/S1040-6182(98)00056-1.

Kuuskraa, V., Stevens, S., Van Leeuwen, T., and Moodhe, K., 2011, World Shale Gas Resources: An Initial Assessment of 14 Regions Outside the United States: Arlington, Virginia, Advanced Resources International, 353 p.

Lambiase, J.J., 1990, A model for the tectonic control of lacustrine stratigraphic sequences in continental rift basins, *in* Katz, B.J., ed., Lacustrine Exploration: Case Studies and Modern Analogues: American Association of Petroleum Geologists Memoir 50, p. 265–276.

Latrubesse, E.M., Stevaux, J.C., Cremon, E.H., May, J.-H., Tatumi, S.H., Hurtado, M.A., Bezada, M., and Argollo, J.B., 2012, Late Quaternary megafans, fans and fluvio-aeolian interactions in the Bolivian Chaco, Tropical South America: Palaeogeography, Palaeoclimatology, Palaeoecology, v. 356-357, p. 75–88, doi:10.1016/j.palaeo.2012.04.003.

Lawton, T.F., 2008, Laramide sedimentary basins, *in* Miall, A.D., ed., The Sedimentary Basins of the United States and Canada: Sedimentary Basins of the World, Volume 5: Amsterdam, Elsevier, p. 431–452, doi:10.1016/S1874-5997(08)00012-9.

Martínez, D.E., 1995, Changes in the ionic composition of a saline lake, Mar Chiquita, province of Córdoba, Argentina: International Journal of Salt Lake Research, v. 4, p. 25–44, doi:10.1007/BF01992412.

Martínez, D.E., Gómez Peral, M., and Maggi, J., 1994, Caracterización geoquímica y sedimentológica de los fangos de la laguna Mar Chiquita, Provincia de Córdoba: aplicación del análisis multivariante: Revista de la Asociación Geológica Argentina, v. 49, p. 26–38.

McGlue, M.M., Scholz, C.A., Karp, T., Ongodia, B., and Lezzar, K.-E., 2006, Facies architecture of flexural margin lowstand delta deposits in Lake Edward, East African rift: Constraints from seismic reflection imaging: Journal of Sedimentary Research, v. 76, p. 942–958, doi:10.2110/jsr.2006.068.

McGlue, M.M., Silva, A., Corradini, F.A., Zani, H., Trees, M.A., Ellis, G.S., Parolin, M., Swarzenski, P.W., Cohen, A.S., and Assine, M.L., 2011, Limnogeology in Brazil's "Forgotten Wilderness": A synthesis from the floodplain lakes of the Pantanal: Journal of Paleolimnology, v. 46, p. 273–289, doi:10.1007/s10933-011-9538-5.

McGlue, M.M., Ellis, G.S., Cohen, A.S., and Swarzenski, P.W., 2012, Playa-lake sedimentation and organic matter accumulation in an Andean piggyback basin: The recent record from the Cuenca de Pozuelos, north-west Argentina: Sedimentology, v. 59, p. 1237–1256, doi:10.1111/j.1365-3091.2011.01304.x.

Meyers, P.A., and Teranes, J.L., 2001, Sediment organic matter, *in* Last, W.M., and Smol, J.P., eds., Tracking Environmental Change Using Lake Sediments. Volume 2, Physical and Geochemical Methods: Springer Developments in Paleoenvironmental Research, Volume 2, p. 239–269.

Mon, R., and Gutiérrez, A.A., 2009, The Mar Chiquita Lake: An indicator of intraplate deformation in the central plain of Argentina: Geomorphology, v. 111, p. 111–122, doi:10.1016/j.geomorph.2009.04.009.

Moore, D.M., and Reynolds, R.C., Jr., 1989, X-ray Diffraction and the Identification and Analysis of Clay Minerals: New York, Oxford University Press, 132 p.

Nemčok, M., Schamel, S., and Gayer, R., 2005, Thrustbelts—Structural Architecture, Thermal Regimes and Petroleum Systems: New York, Cambridge University Press, 541 p.

Nores, M., 2011, Long-Term Waterbird Fluctuations in Mar Chiquita Lake, central Argentina: Waterbirds, v. 34, p. 381–388, doi:10.1675/063.034.0314.

Peel, M.C., Finlayson, B.L., and McMahon, T.A., 2007, Updated world map of the Köppen-Geiger climate classification: Hydrology and Earth System Sciences, v. 11, p. 1633–1644, doi:10.5194/hess-11-1633-2007.

Pelletier, J.D., 2007, Erosion-rate determination from foreland basin geometry: Geology, v. 35, p. 5–8, doi:10.1130/G22651A.1.

Peters, K.E., 1986, Guidelines for evaluating petroleum source rock using programmed pyrolysis: American Association of Petroleum Geologists Bulletin, v. 70, p. 318–329.

Piovano, E.L., Ariztegui, D., and Damatto Moreira, S., 2002, Recent environmental changes in Laguna Mar Chiquita (central Argentina): A sedimentary model for a highly variable saline lake: Sedimentology, v. 49, p. 1371–1384, doi:10.1046/j.1365-3091.2002.00503.x.

Piovano, E.L., Ariztegui, D., Bernasconi, S.M., and McKenzie, J.A., 2004, The isotopical record of hydrological changes in subtropical South America over the last 230 years: The Holocene, v. 14, p. 525–535, doi:10.1191/0959683604hl729rp.

Pollastro, R.M., Jarvie, D.M., Hill, R.J., and Adams, C.W., 2007, Geologic framework of the Mississippian Barnett Shale, Barnett-Paleozoic total petroleum system, Bend arch–Fort Worth Basin, Texas: The American Association of Petroleum Geologists Bulletin, v. 91, p. 405–436, doi:10.1306/10300606008.

Rahman, M., and Kinghorn, R.R.F., 1995, A practical classification of kerogens related to hydrocarbon generation: Journal of Petroleum Geology, v. 18, p. 91–102, doi:10.1111/j.1747-5457.1995.tb00743.x.

Ramos, V.A., Cristallini, E.O., and Pérez, D.J., 2002, The Pampean flat slab of the Central Andes: Journal of South American Earth Sciences, v. 15, p. 59–78, doi:10.1016/S0895-9811(02)00006-8.

Reati, G.J., Florín, M., Fernández, G.J., and Montes, C., 1996, The Laguna de Mar Chiquita (Cordoba, Argentina): A little known, secularly fluctuating, saline lake: International Journal of Salt Lake Research, v. 5, p. 187–219, doi:10.1007/BF01997137.

Roberts, S.B., 2005, Geologic assessment of undiscovered petroleum resources in the Wasatch–Green River composite total petroleum system, southwestern Wyoming province, Wyoming, Colorado, and Utah, *in* USGS Uinta-Piceance Assessment Team, compilers, Petroleum systems and geologic assessment of oil and gas in the southwestern Wyoming province, Wyoming, Colorado, and Utah: U.S. Geological Survey Digital Data Series DDS–69-D, 26 p.

Roehler, H.W., 1993, Correlation, composition, areal distribution, and thickness of Eocene stratigraphic units, greater Green River basin, Wyoming, Utah, and Colorado: U.S. Geological Survey Professional Paper 1506E, 49 p.

Ross, D.J.K., and Bustin, R.M., 2007, Shale gas potential of the Lower Jurassic Gordondale Member, northeastern British Columbia, Canada: Bulletin of Canadian Petroleum Geology, v. 55, p. 51–75, doi:10.2113/gscpgbull.55.1.51.

Ross, D.J.K., and Bustin, R.M., 2009, The importance of shale composition and pore structure upon gas storage potential of shale gas reservoirs: Marine and Petroleum Geology, v. 26, p. 916–927, doi:10.1016/j.marpetgeo.2008.06.004.

Santini, K., Fastert, T., and Harris, R., 2006, Soda ash, *in* Kogel, E.J., Trivedi, N.C., Barker, J.M., and Krukowski S.T., eds., Industrial minerals and rocks: Commodities, markets, and uses (seventh edition): New York, Society for Mining, Metallurgy, and Exploration, p. 1584.

Singh, B.P., Andotra, D.S., and Kumar, R., 2000, Provenance of the lower Tertiary mudrocks in the Jammu Sub-Himalayan zone, Jammu and Kashmir State (India), NW Himalaya, and its tectonic implications: Geosciences Journal, v. 4, p. 1–9, doi:10.1007/BF02910208.

Sladen, C.P., 1994, Key elements during the search for hydrocarbons in lake systems, *in* Gierlowski-Kordesch, E.H., and Kelts, K.R., eds., Global Geological Record of Lake Basins Volume 1: Cambridge, UK, Cambridge University Press, p. 3–17.

Smith, M.E., Carroll, A.R., and Singer, B.S., 2008, Synoptic reconstruction of a major ancient lake system: Eocene Green River Formation, western United States: Geological Society of America Bulletin, v. 120, p. 54–84, doi:10.1130/1326073.1.

Smoot, J.P., and Lowenstein, T.K., 1991, Depositional environments of nonmarine evaporites, *in* Melvin, J.L., ed., Evaporites, Petroleum and Mineral Resources: Developments in Sedimentology Volume 50: Amsterdam, Elsevier, p. 189–347.

Surdam, R.C., and Stanley, K.O., 1979, Lacustrine sedimentation during the culminating phase of Eocene Lake Gosiute, Wyoming (Green River Formation): Geological Society of America Bulletin, v. 90, p. 93–110, doi:10.1130/0016-7606(1979)90<93:LSDTCP>2.0.CO;2.

Talbot, M.R., 2001, Nitrogen isotopes in palaeolimnology, *in* Last, W.M., and Smol, J.P., eds., Tracking Environmental Change Using Lake Sediments. Volume 2, Physical and Geochemical Methods: Springer Developments in Paleoenvironmental Research, Volume 2, p. 401–439.

Talbot, M.R., and Johannessen, T., 1992, A high resolution palaeoclimatic record for the last 27, 500 years in tropical West Africa from the carbon and nitrogen isotopic composition of lacustrine organic matter: Earth and Planetary Science Letters, v. 110, p. 23–37, doi:10.1016/0012-821X(92)90036-U.

Troin, M., Vallet-Coulomb, C., Sylvestre, F., and Piovano, E., 2010, Hydrological modeling of a closed lake (Laguna Mar Chiquita, Argentina) in the context of 20th century climatic changes: Journal of Hydrology (Amsterdam), v. 393, p. 233–244, doi:10.1016/j.jhydrol.2010.08.019.

Valero-Garcés, B.L., Delgado-Huertas, A., Ratto, N., Navas, A., and Edwards, L., 2000, Paleohydrology of Andean saline lakes from sedimentological and isotopic records, northwestern Argentina: Journal of Paleolimnology, v. 24, p. 343–359, doi:10.1023/A:1008146122074.

Varandas da Silva, L.S., Piovano, E.L., Azevedo, D.A., and Aquino Neto, F.R., 2008, Quantitative evaluation of sedimentary organic matter from Laguna Mar Chiquita, Argentina: Organic Geochemistry, v. 39, p. 450–464, doi:10.1016/j.orggeochem.2008.01.002.

Vörösmarty, C.J., Routhier, M., Wright, A., Baker, T., Fernandez-Jauregui, C.A., and Donoso, M.C., 1998, A Regional Hydrometeorological Data Network for South America, Central America, and the Caribbean (R-HydroNET v1.0), http://www.r-hydronet.sr.unh.edu/.

Wentworth, C.K., 1922, A scale of grade and class terms for clastic sediments: Journal of Geology, v. 30, p. 377–392, doi:10.1086/622910.

Wirrmann, D., and Mourguiart, P., 1995, Late Quaternary spatio-temporal limnological variations in the Altiplano of Bolivia and Peru: Quaternary Research, v. 43, p. 344–354, doi:10.1006/qres.1995.1040.

Zaleha, M.J., 2006, Sevier orogenesis and nonmarine basin filling: Implications of new stratigraphic correlations of Lower Cretaceous strata throughout Wyoming, USA: Geological Society of America Bulletin, v. 118, p. 886–896, doi:10.1130/B25715.1.

Zanor, G.A., Piovano, E.L., Ariztegui, D., and Vallet-Coulomb, C., 2012, A modern subtropical playa complex: Salina de Ambargasta, central Argentina: Journal of South American Earth Sciences, v. 35, p. 10–26, doi:10.1016/j.jsames.2011.10.007.

Zhang, T.W., Ellis, G.S., Ruppel, S.C., Milliken, K., and Yang, R.S., 2012, Effect of organic matter type and thermal maturity on methane adsorption in shale-gas systems: Organic Geochemistry, v. 47, p. 120–131, doi:10.1016/j.orggeochem.2012.03.012.

Manuscript Accepted by the Society 30 March 2015

Printed in the USA

Geological Society of America Special Papers Online First

Modern muds of Laguna Mar Chiquita (Argentina): Particle size and organic matter geochemical trends from a large saline lake in the thick-skinned Andean foreland

Michael M. McGlue, Geoffrey S. Ellis and Andrew S. Cohen

Geological Society of America Special Papers, published online August 6, 2015;
doi:10.1130/2015.2515(01)

Notes